HOST UNIVERSITY: The University of Edinburgh

FACULTY: College of Science and Engineering

DEPARTMENT: School of Engineering

Academic Year 2020-2021

IS THERE A VERTICAL TRENCH EFFECT?

Anna Gorodilova

Supervisor: Dr Ricky Carvel

Master thesis submitted in the Erasmus+ Study Programme

International Master of Science in Fire Safety Engineering

Disclaimer

This thesis is submitted in partial fulfilment of the requirements for the degree of *The International Master of Science in Fire Safety Engineering (IMFSE)*. This thesis has never been submitted for any degree or examination to any other University/programme. The author(s) declare(s) that this thesis is original work except where stated. This declaration constitutes an assertion that full and accurate references and citations have been included for all material, directly included and indirectly contributing to the thesis. The author(s) gives (give) permission to make this master thesis available for consultation and to copy parts of this master thesis for personal use. In the case of any other use, the limitations of the copyright have to be respected, in particular with regard to the obligation to state expressly the source when quoting results from this master thesis. The thesis supervisor must be informed when data or results are used.

Read and approved,

Anna Gorodilova

May 11th, 2021

Main body word count: 16103

Abstract

Series of experiments was carried out with and without trench sidewalls on PMMA (Polymethylmethacrylate) samples in order to investigate flame spread physics influenced by a fuel geometry. It was determined that the so-called “trench effect” was investigated extensively only several decades ago where the main focus of the studies was on angles below 45 degrees. This research is mainly focused on the flame spread behaviour at steep angles between 50 and 90 degrees in a trench to expand upon previous studies found in literature. Video data analysis was the main tool for measurements, however, series of thermocouples were installed along the centerline of a sample as a point of comparison.

The results showed that the flame spread rate in a trench grows sharply between 15 and 30 degrees, but then remained almost constant at angles from 50 to 90 degrees even if the height of sidewalls were varied. This behaviour is completely different when sidewalls are absent since the flame spread rate demonstrated a gradual growth with an increase of inclination angle. Also, the presence of sidewalls greatly influences both flame spread rate and its structure that was observed during the tests. Flame and pyrolysis front shapes were compared and discussed in detail where possible influential factors on the contour were mentioned.

In addition, the findings from this work can contribute to a better understanding of the flame spread topic in general and propose some questions for further research.

Аннотация

В данной работе была проведена серия экспериментов с образцами в виде желоба с ПММА (Полиметилметакрилат) материалом в качестве горючего, а также с образцами без боковых стенок, для изучения влияния геометрии горючего на физику распространения пламени. Выяснилось, что так называемый «эффект желоба» широко исследовался только несколько десятилетий назад, где основное внимание уделялось образцам, наклоненным ниже 45 градусов. Данное исследование сосредоточено на изучении распространения пламени при крутых углах от 50 до 90 градусов. Анализ видеоданных был основным инструментом для измерений, однако ряд термопар был установлен вдоль центральной линии тестируемого образца для сравнения результатов от двух источников.

Результаты показали, что скорость распространения пламени в желобе резко возрастает между 15 и 30 градусами, но затем остается почти низменной при углах от 50 до 90 градусов, даже если высота боковых стенок изменяется. При отсутствии боковых стенок, поведение пламени было совершенно иным, так как скорость распространения огня возрастала равномерно с увеличением угла наклона. Кроме того, наличие боковых стенок сильно влияет как на скорость распространения пламени, так и на его форму, что было замечено во время испытаний. Также проведено сравнение формы пламени и формы пиролиза на образце, где возможные факторы, влияющие на эту форму, были обсуждены.

Результаты этой работы могут поспособствовать большему пониманию темы распространения пламени в целом и в частности предложить некоторые вопросы для дальнейших исследований.

Acknowledgments

I would like to express my gratitude to people from the IMFSE programme that allowed me to grow as an engineer and learn a lot about Fire Safety in general. Thanks to all three universities each of them provided a unique environment and learning opportunities that greatly contributed to my knowledge and made it possible to write this thesis.

I am grateful to my supervisor Dr. Ricky Carvel who helped me to perform this work. Also thanks to his guidance and helpful remarks throughout this semester.

I would like to thank Dougal Drysdale for an opportunity to discuss the trench effect topic in person.

Special thanks to David Morrisset for his endless support in the lab and contagious enthusiasm that charged me whenever I talked with him.

I would also like to thank all people in the John Muir building who aided me to conduct my experiments and who helped me to socialize after tough isolation times at home.

Great and warm thanks to my family and friends for their strong support and patience during my master's studies. Very special gratitude goes to my mother and Sasha who motivated and supported me every day and even if sometimes we were far from each other.

Table of Contents

List of Figures

List of Tables

Notation

Latin symbols

A_T – trench aspect ratio (-)

A_B – ratio between the width of the burner and the width of the trench (-)

a_p – acceleration of the pyrolysis front (mm/s^2)

c – specific heat capacity (J/kgK)

D – characteristic dimension (m)

F_{buoy} – buoyancy force (N)

$F_{buoy,p}$ – perpendicular buoyancy force (N)

$F_{buoy,n}$ – normal buoyancy force (N)

F_{12} – view factor between flame and surface (-)

g – acceleration due to gravity (m/s^2)

ΔH – enthalpy increase per unit mass of fuel (J/kg)

h – convective heat transfer coefficient (W/m^2K)

h_g – effective heat of gasification (J/kg)

h_{melt} – heat of melting (J/kg)

h_{vap} – heat of vaporization (J/kg)

h_{pyr} – heat of pyrolysis (J/kg)

k – thermal conductivity (W/mK)

L – thickness of the fuel (m)

$\dot{m}''$ – mass loss rate per unit area of the fuel (g/cm^{2}s)

$\dot{Q}'$ –heat release rate per unit length (W/cm)

q – heat released per unit mass of the fuel consumed (J/kg)

$\dot{q}''$ – amount of energy provided to the pyrolysis region (W/m^2)

$\dot{q}''_{ig}$ – required heat flux to ignite the surface (W/m^2)

$\dot{q}''_{loss}$ – heat losses from the surface (W/m^2)

$\dot{q}''_{fl}$ – heat coming from the flames to the virgin fuel (W/m^2)

$\dot{q}''_{rad}$ – radiation (W/m^2)

$\dot{q}''_{conv}$ – convection (W/m^2)

$\dot{q}''_{rr}$ – reradiation from the surface (W/m^2)

$\dot{q}''_{ref}$ – reflection from the surface based on the material reflectivity (W/m^2)

$\dot{q}''_{id,rad}$ – in-depth radiation (W/m^2)

$\dot{q}''_{id,cond}$ – in-depth conduction (W/m^2)

T – temperature (K)

T_p – pyrolysis temperature (K)

T_a – ambient temperature (K)

T_0 – initial temperature (K)

T_f – flame temperature (K)

T_s – surface temperature (K)

t – time (s)

U – Velocity of the gases (m/s)

V_p – velocity of the pyrolysis front (m/s)

w – width (m)

x – depth of the heating layer (m)

x_f – flame length (m)

x_p – pyrolysis front length (m)

Greek symbols

α – thermal diffusivity (m^2/s)

α_r – absorptivity (-)

ε_f – emissivity of the flame (-)

ε_s – emissivity of the fuel surface (-)

σ – Stefan-Boltzmann constant (W/m^2K^4)

δ – thermal penetration depth (m)

δ_s – preheated length (m)

ρ – fuel density (kg/m^3)

ρ_r – reflectivity (-)

τ – characteristic time for ignition (s)

τ_r – transmissivity (-)

Ж – relative change of velocity and acceleration parameter (-)

Chapter 1 Introduction

In the modern rapidly developing world we are surrounded by a variety of materials that usually constitute structures with complex designs and shapes. From the perspective of fire safety, these structures can be considered as potential hazards that in case of fire may pose a threat to life and property. Therefore, compromising the main goals in fire safety [1]. Also, the materials that were used for the design are perceived as combustibles that can have multiple fire behaviour patterns depending on the conditions, in other words, they are system dependent. For example, the same fuel can burn differently in changing oxygen concentrations, ambient pressure, external radiation, inclined angle and fuel geometry [2]. The last two options are the focus of this study. In general, the flame spread over the surfaces is a crucial determinant of the fire severity, since the flame spread over the solids determines the rate at which fire can grow and further involve more fuels. Some of the flame spread regimes can be very disruptive, particularly concurrent flame spread over solids on inclined surfaces, that is one of the most threatening configurations [2]. This regime can be more rapid in a specific restrained geometry, for instance in partly enclosed channels or trenches. This work is devoted to the investigation of flame spread behaviour in laboratory-scale trench-like structures at different inclination angles. A sufficient understanding of the trench effect phenomenon is vital for the final design evaluation that contains similar geometrical features. Also, it is important to know the potential threats and have a clear understanding of how to mitigate the risks connected with this type of flame spread.

1.1 Historical background

The King's Cross Fire disaster is an example of how insufficient knowledge of flame spread mechanisms can lead to numerous fatalities in a very short time. The accident occurred in the evening on Wednesday 18 November 1987 at King's Cross Underground Station, London, UK. This station was the busiest transportation hub in 1987 that had five different levels under the ground and various connections by passageways, staircases and escalators. Three notorious escalators at King's Cross between the Piccadilly Line and the ticket hall were installed in 1939 and made mainly of wood. They were inclined at 30 degrees and were 17.2 meters long forming a very long trench structure. The fire started from small flame and it took just 15 minutes to evolve to a flashover stage. This resulted

in a fast and abrupt jet of flames in the upper part of the escalator that rushed rapidly and killed 31 people [3].

After the initiation of a public inquiry, a lot of work was done by experts in order to investigate and comprehend the reasons for such rapid flame spread along the escalator line. Moodie et al. [4] investigated that flame acceleration in the inclined escalator trench occurred due to the influence of aerodynamics effects that enhance preheating of the wood and further ignition. It was discovered that upward fire acceleration and eruption into the ticket hall was induced by a phenomenon called the “trench effect” which occurs only in partly enclosed inclined channels and can be dangerous due to the unpredictably high rate of the flame spread [3].

It should be noted that not only elevated escalator stairs can be a potential source of this phenomenon, but also any inclined structure that has a U-shape and contains combustible materials. For example, forest terrain can have natural upslope trenches which in the case of a forest fire may quickly facilitate the spread of the fire and escalate the danger. Viegas et al. [5] considered some examples of forest fire blow-up due to the existence of a steep slope in a canyon terrain that resembles a trench. This relief configuration in case of fire led to numerous deaths and enormous damage due to the unexpectedly high velocity of flames in most of the discussed occasions. Also, Sharples et al. [6] likened eruptive fire behaviour in forests with the King’s Cross accident, noting that the investigation and prediction of trench effect phenomenon are vital not only for dwellings but also for firefighters, who are always in direct contact with fire. In addition, Chen et al [7] reported that in trench-like terrain a forest fire in China killed 30 people in 2019. Another disaster caused by trench geometry occurred in 2015 in China, where 21 coal mine workers were killed by a fast fire that originated in a long conveyor belt that was inclined at a steep angle [8]. The trench effect is also seen in large-scale U-shaped facades. It was shown by Yan Weigang et al. [9] that sidewalls greatly enhance the upward flame spread along the façade and this geometrical configuration requires a lot of attention from an engineering design perspective for a higher level of fire safety of buildings containing such architectural feature. The phenomenon of a trench effect takes place in a variety of instances and has to be studied adequately to prevent such catastrophic events with fatalities.

1.2 Flame spread definition

The fundamental physics of solid flame spread must first be discussed before outlining the trench effect in detail. To begin with, flame spread is a process of flame propagation with a certain velocity that has direct contact with a heated surface that acts as a fuel source. There are two main mechanisms according to Hirano et al. [10] that must happen in order to observe the flame spread phenomenon. The primary mechanism is a sufficient heat transfer from the flaming region to the virgin material that raises the temperature from ambient to its vaporization value. Afterward, released pyrolysis gases must react with the gaseous oxidizer to propagate further and maintain the flame spread process. Figure 1 depicts a schematic diagram of a flame propagation process of an opposed flow flame spread (or counter-current) on a horizontal surface that is characterized by the flame front progressing in the opposite direction from the ambient flow environment.

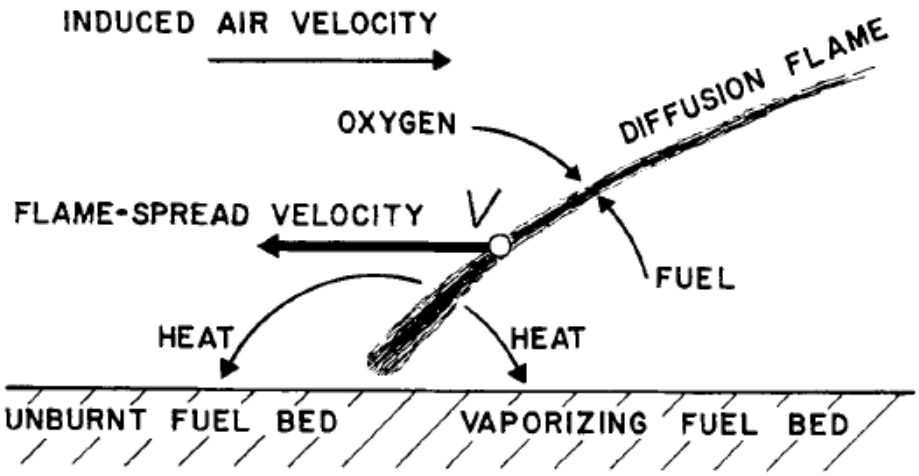

Figure 1. Schematic diagram of natural flame spread from de Ris et al. work [11]

Numerous studies exist outlining flame spread in a mathematical form, but the most fundamental equation was written by Williams et al. [12] that can be used to describe fire spread physics by a simple energy conservation equation:

$$\rho V_p \Delta H = \dot{q}'' \quad (1)$$

Judging by the formula, the main requirement for the flame spread is the amount of energy transferred to the virgin surface shall be enough to heat the surface to its pyrolysis temperature. If the amount of heat is insufficient, the flame spread will not occur. This equation can be used for different flame spread problems, where the most complicated parameter to determine is the dominant heat transfer mechanism. In order to reveal a

major flame spread mechanism that produces the largest velocity, it is important to understand which factors can influence this process [13]. Drysdale et al. [14] provide a list of factors that could affect the rate of flame spread over combustible solid that can be seen in Table 1 below.

Table 1. Factors affecting flame spread [14]

Material factors		Environmental factors
Chemical	Physical	
Composition of fuel Presence of retardants	Initial temperature Surface orientation Direction of propagation Thickness Thermal capacity Thermal conductivity Density Geometry Continuity	Composition of atmosphere Pressure of atmosphere Temperature Imposed heat flux Air velocity

It should be noted that in this study the main focus was only on physical material factors, namely surface orientation, the direction of propagation, thickness and geometry. They will be discussed further in this work.

The simplest example of a surface flame spread is a horizontal flame spread in a quiescent environment. Heat transfer from the flame to an unburnt surface occurs primarily by means of radiation and conduction in this case [15]. Additionally, Fernandez-Pello et al. [10] found that for the smaller thickness conduction through the gas phase is dominant, while for a thicker fuel the conduction through the solid phase becomes substantial as well. In another study [16] they observed that radiation becomes more important with the increasing the fire size. Also, there is no convective forward heat transfer due to the presence of opposed air entrainment even though the process occurs in the still environment [11]. For better understanding Fig. 2 shows a schematic diagram of heat transfer processes that occurs on a horizontal surface. It should be noted that the char layer appears only in the case of charring materials, for example, wood.

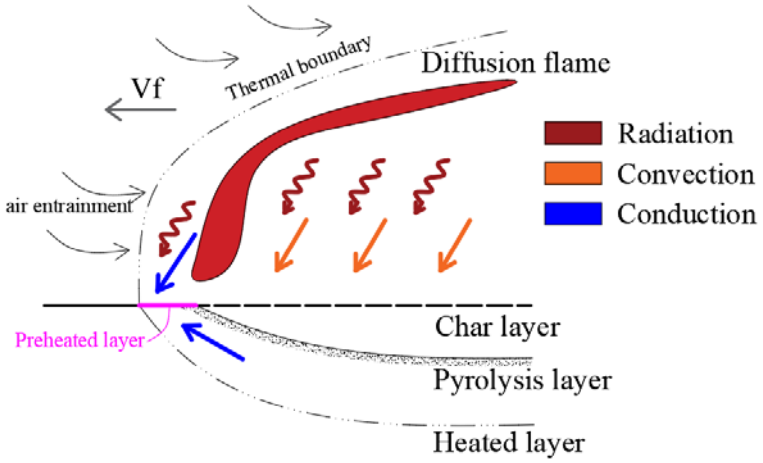

Figure 2. Heat transfer process on a horizontal surface

1.3 Flame spread on an inclined surface

The flame behaviour changes considerably when an inclined surface is used instead of horizontally oriented. Wu et al. [17] conducted some experiments to study the influence of slope on the behaviour of the flames. The first observation that was made is that the flame starts to tilt towards the fuel surface with an increase of the inclination angle of the fuel bed. Figure 3 shows a schematic representation of the flame tilting on the inclined surface.

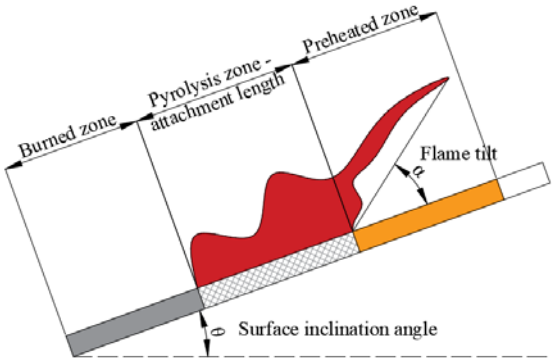

Figure 3. Flame tilting diagram

When the sample was inclined to 26°, the flame attachment length starts to increase rapidly, changing from steady-state to an accelerative flame spread mode. This inclination value can be called the "critical inclination angle" at which the spread rate increases rapidly over a surface. According to Zhang et al. [18] work, the critical angle was in between 10°-20° and this zone, at which acceleration of flame spread rate occurs, is called a "transition zone".

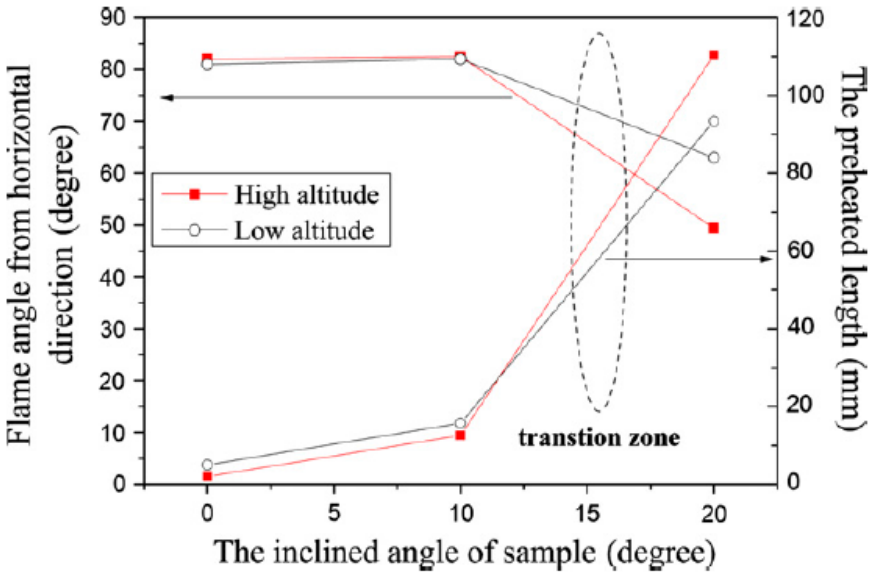

Figure 4. Transition zone in the inclined surface [18]

Figure 4 depicts the results from Zhang et al. experiments on whitewood, where the transition zone is circled. It can be seen that the preheated length starts to increase sharply after 10° while the flame tilting angle drops down with an increase of the angle of the sample.

Several factors are responsible for such a rapid transition. First of all, the critical angle indicates that a fundamental change in both fluid mechanics and heat transfer occurs. The flame spread switches from counter-current to concurrent mode that indicates a much faster flame spread [14]. This means that hot gas flow moves in the same direction with the flame spread thereby pushing hot gases ahead towards the virgin fuel area. These gases in combination with increased view factor improve the transfer of the heat from flames to the unburnt region, therefore increasing the spread rate [10]. The resulting flame spread is more rapid and hazardous than counter-current flame spread, thus upward flame spread is of greater interest in this study. Figure 5 shows a schematic diagram for concurrent (or wind-aided) flame spread mode. It can be observed that the rate of flame spread will depend on how quickly the virgin surface temperature is heated to its vaporization temperature. In turn, it depends on the flame length and heat flux coming from the flames to the virgin fuel.

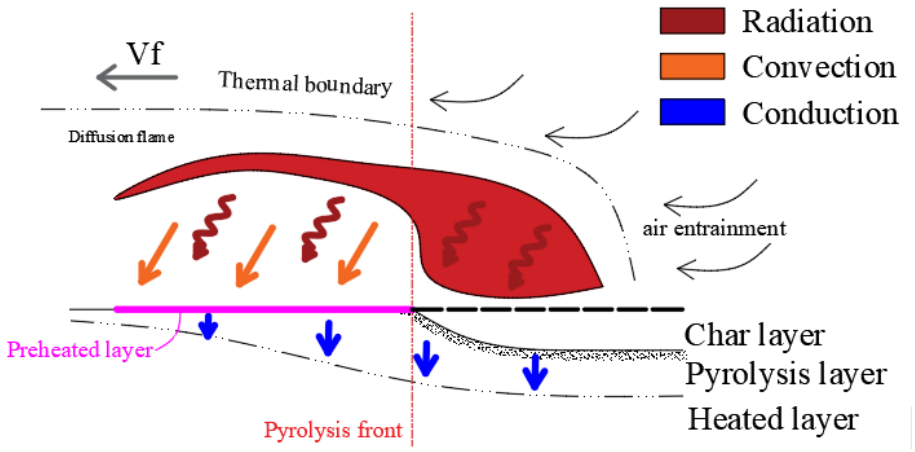

Figure 5. Concurrent flame spread after a critical angle

The experiment with upward flame spread conducted by Orloff et al.[19] revealed that the spread is laminar only in the beginning of the burning region, where the convection is the dominant mechanism. Approximately after 10 cm, the fire becomes fully turbulent and radiation is considered to be the dominant mode of the heat transfer constituting about 80% of the total heat transfer. These findings are consistent with Fernandez-Pello et al. [16] research, who also observed that a flow-assisted flame spread is mostly turbulent where radiation from fire to the unburnt fuel plays an important role in the heat transfer process, however, convection also should be taken into account. According to Hasemi et al. [20], the wall heat flux is governed by convection only in the far-field region.

Upward flame spread is not steady due to a "positive feedback loop" that was well explained by Beji et al. [15]. Improved heat transfer due to the switch to the concurrent flow increases the burning area from which volatiles are released. Then, the larger burning area produces a larger heat release rate and consequently even larger flames. All these processes induce the more severe and extensive preheating of the virgin fuel and its further faster ignition and contribution to the fire spread. These findings are in good agreement with Fernandez-Pello et al. [10], who mentioned that the rate of flame spread is dependent on how quickly the unburnt fuel surface will be heated to its ignition temperature. Quintiere et al. [21] described the vertical flame spread rate V_p over thermally thick fuel by the following approximation assuming that heat flux $\dot{q}''_{ig}$ remains relatively constant across a preheated zone length δ_s during flame spread procces:

$$V_p = \frac{4(\dot{q}''_{ig})^2(x_f - x_p)}{\pi k \rho c (T_p - T_a)^2} \qquad (2)$$

Quintiere et al. [22] explains the presence of $\pi/4$ as an assumption that incident heat flux from the flames to the surface is quasi-constant over the flame extension region and becomes zero when $x > x_f$. In addition, Quintiere [23] provides an expression for characteristic time for ignition τ that specified below:

$$\tau = \frac{\pi}{4} k\rho c \left[\frac{T_p - T_a}{\dot{q}''_{ig}}\right]^2 \tag{3}$$

It can be seen that τ is dependent on the incident heat flux from the flames and when the flames are larger, the heat flux is also larger. This means that the characteristic time for ignition will be lower resulting in a faster flame spread. Also, the time required for ignition depends on fuel properties and ambient temperature. The lower thermal inertia of a material, for example insulation foams, results in faster ignition and propagation of the flame front.

So finally, Eq. 2 can be rewritten in the shorter form:

$$V_p \sim \frac{\delta_s}{\tau} \sim \frac{x_f - x_p}{\tau} \tag{4}$$

Also, from Drysdale [14] it was found that flame spread rate is dependent on the length of the pyrolysis zone, which determines the extent of the preheating zone, and can be expressed in the following correlation:

$$V_p \propto x_p^n \tag{5}$$

However, there is another important effect that is responsible for the strong flame attachment and further flame spread acceleration. According to Grumstrup et al. [24], there is an inequality of air entrainment from the upslope and downslope sides when the surface is inclined. The reduced entrainment from the upper side bends the flame towards the surface due to the influence of a greater momentum from the underside. Figure 6 from this work helps to understand this phenomenon better. It can be observed, the buoyancy force F_{buoy} is divided on two components: $F_{buoy,p}$ that facilitates uphill entrainment and $F_{buoy,n}$. With increase of the surface inclination angle, the component $F_{buoy,p}$ rises, supressing downhill entrainment.

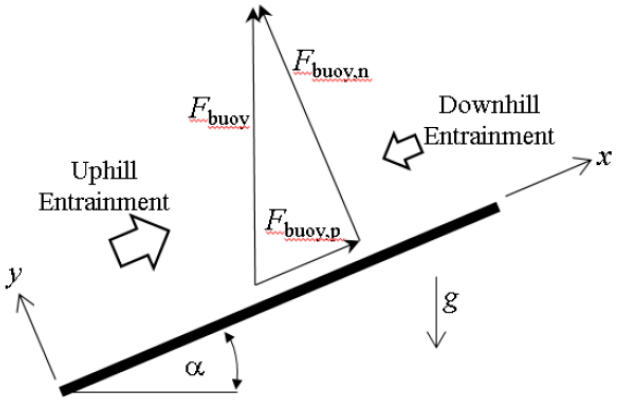

Figure 6. Buoyancy vector decomposition [24]

At some critical angle that was described above, downhill entrainment becomes negligibly small, thus the fire plume attaches to the surface completely, essentially increasing the preheated length of the virgin fuel and accelerating further propagation of the flame. This effect is also called the "Coanda effect" that appears due to the pressure gradient induced by differences of the air entrainment from the upslope and downslope side [25].

1.4 Fire in an inclined trench

With the presence of the sidewalls on inclined surfaces, the flame behaves quite differently due to the appearance of several factors. First of all, a channel geometry prevents lateral air entrainment to the fire source. Without sidewalls, the flame can entrain air from all available sides. However, when walls are mounted, the only possible directions of the entrainment are front and bottom sides. (see Fig 7). This is an important requirement for the trench effect phenomenon that air can be entrained only along the plane of the inclination and not perpendicular to it, forming two-dimensional flow.

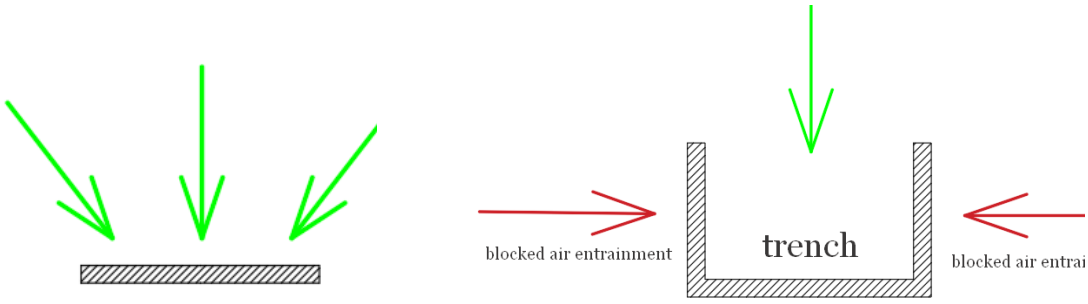

Figure 7. The difference in air entrainment within the trench and outside it

In addition, Woodburn et al. explained the consequences of a fire in such channels. Figure 8 demonstrates the difference in air inflow within the trench and outside it. Due to the large inequality between the momentum of entrained air between downslope and upslope parts in the two-dimensional flow, the fire plume deflects towards the channel much stronger than in the case of a free plume. This is because the free plume is unrestricted from all sides and even the same large imbalance in the momentum (same angle) has less influence on the deflection of the plume [26].

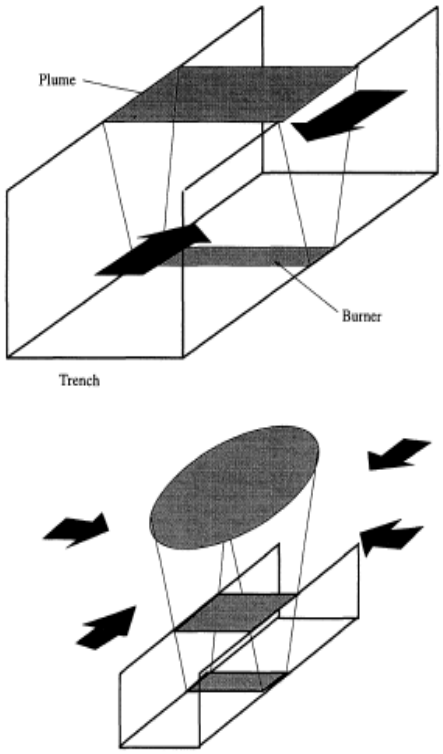

Figure 8. 2D and 3D plumes [26]

Moreover, Simcox et al. [27] conducted numerical modeling of the King's Cross escalator fire that allowed to reveal two main aerodynamic effects that in combination are responsible for the trench effect. Firstly, simulation results showed a considerable chimney effect caused by a heat source that strengthens airflow along the trench. The second responsible factor is the Coanda effect that becomes more tangible in a trench geometry, sticking the flame to the surfaces of the trench [28]. The presence of these aerodynamic phenomena significantly increases the flame length thereby causing the additional preheating length of the fuel in an upward direction and faster flame spread [29].

According to Yan et al. experiments, [9] the more air entrained from the bottom due to restrictions from lateral sides, the higher the speed of the airflow inside the trench. It means that the increased velocity of the air will facilitate the flame spread along the channel. Additionally, the heat going from the attached plume is partially restricted by the sidewalls which increase the heat feedback to the fuel. In addition, Jagger et al. [30] observed an effect that could explain the jet effect in the upper part of the escalator. This occurs due to the inherent nature of the flame that is propagating in a channel, to curve inward towards the centerline of the trench from two lateral sidewalls. As soon as the flames reached the end of the trench, they emerged with significant momentum parallel to the trench to create a wall jet effect. In addition, unlike the unrestricted inclined flame spread, the dominating heat transfer mode is found to be less pronounced when the fire is in the trench. According to Xie et al. [31], for lower slopes radiative heating is the dominant mechanism, however, convective heat transfer becomes also significant with an increasing slope of the trench due to a stronger channeling effect inside the trench.

As was mentioned before, the higher the inclination angle of the surface, the higher the upward flame spread rate. The same trend can be observed in channels but with a different order of magnitude. After analysis of the available literature, it was found that the most fundamental researches of the trench effect were conducted several years after the King's Cross disaster. For example, Drysdale et al. performed a comprehensive study [32] of fire behaviour in a channel with thick PMMA sheets in order to reveal the trench effect. Figure 10 depicts the results from these experiments where the inclination of the trench was varied from 0° (horizontal) to 90° (vertical). It can be seen that the flame spread rate remained almost constant for all fuel widths until critical 15°-20°. This behaviour is consistent with results from Consalvi et al. [33] who also revealed a very weak influence of inclination angle on the flame spread rate until some critical angular value.

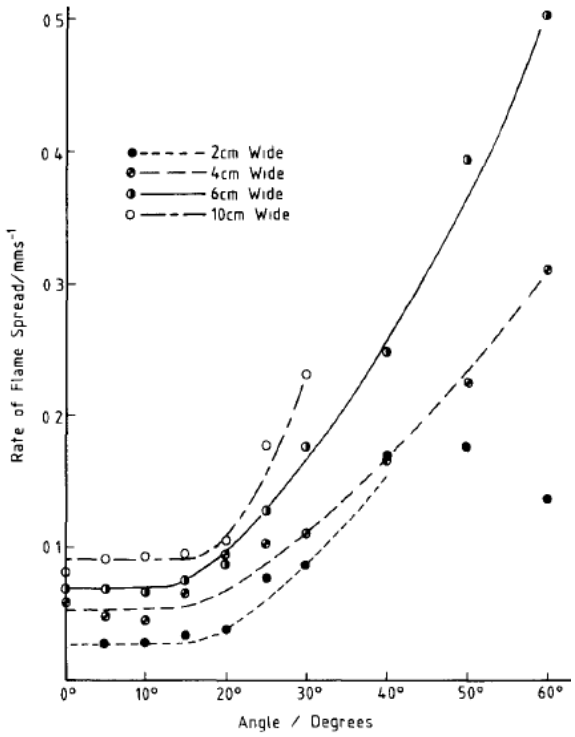

Figure 9. Flame spread rate as a function of inclination angle (no sidewalls) [32]

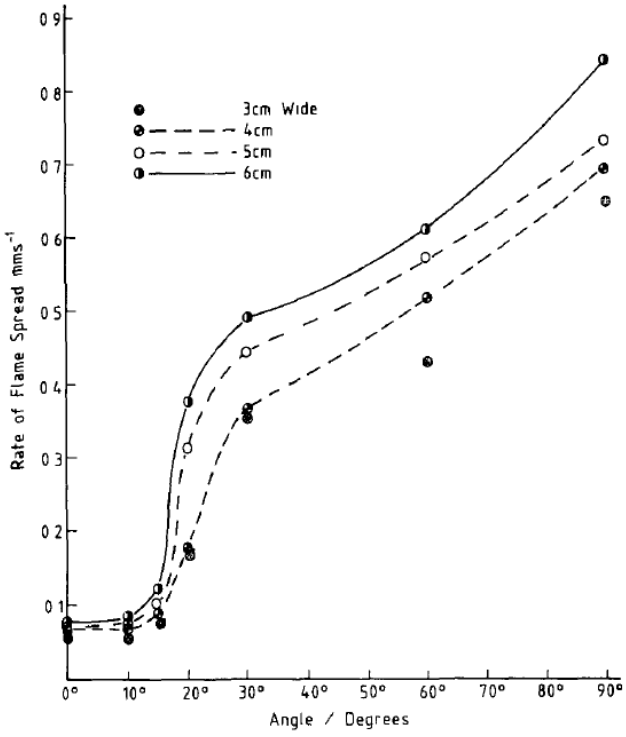

Figure 10. Flame spread rate as a function of inclination angle (with sidewalls) [32]

So, a further increase of the slope shows an abrupt rise in the spread rate. It was observed that at a critical angle of 15°-20° the interaction between flame front and the virgin material changes, inducing enhancement of the heat transfer process. In contrast, the authors did not observe the same acceleration trend in the experiments without sidewalls (Fig. 9), thus the average flame spread rate at 30° was almost five times greater in the trench compared to without sidewalls. Furthermore, Dupuy et al. [34] reported that the flame spread rate at 30° was 10 times higher for 1 m-wide sample with sidewalls than for samples without lateral sides. Drysdale's study also confirms the CFD simulation results conducted by Simcox et al [27] that earlier revealed and explained the trench effect acceleration phenomenon at the King's Cross station. While Yang et al. [28] reported the same critical range 15°-20° for an abrupt increase of flame spread rate in their trench experiments, this parameter is not a fixed value, since other studies show slightly different results. For instance, Smith et al. [35] estimated that the critical angle is equal to 27°, while [34], [36] figured out that rapid acceleration occurs at the angle of 30°. The most surprising results were received by Woodburn et al. [26], who observed that the critical angle varied from 10° to 25° in a set of experiments. It was found that a channel cross-section geometry is an important parameter for flame spread acceleration rate. Also, "the

critical angle depends on how closely the flow in the region below the top of the trench walls approaches two-dimensional flow" [26]. When the trench walls are high enough, they help to create a more pronounced two-dimensional flow and the critical angle tends towards a smaller value.

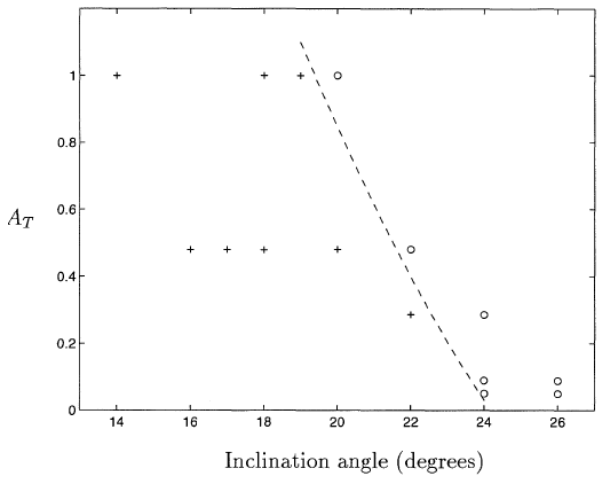

Figure 11. The effect of the trench aspect ratio [26]

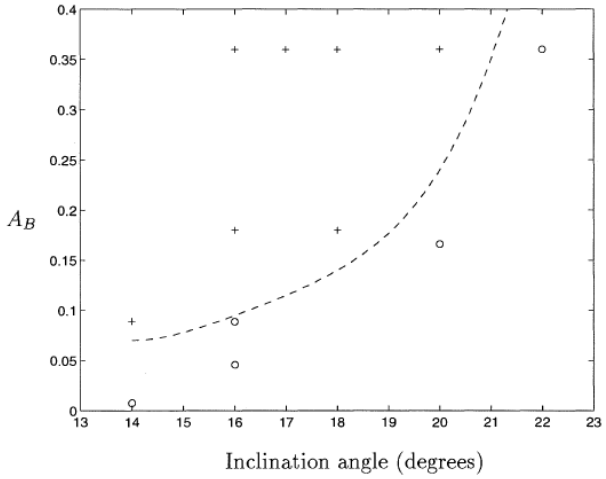

Figure 12. The effect of the burner aspect ratio [26]

Figure 11 shows the critical angle as the function of a trench aspect ratio A_T, where A_T is the ratio between the height and width of the trench. The dashed line represents a boundary between two regimes: vertical plume and attached. As can be observed, the critical angle is lower for higher sidewalls (higher aspect ratio) and vice versa. However, this is not the only finding in the study. The geometry of the burner should be also taken into account during the investigation of the critical angle for the flame acceleration. Figure 12 depicts the critical angle as the function of a burner aspect ratio A_B, where A_B is a ratio between the width of the burner and the width of the trench. It can be seen, that thinner burners decrease the critical angle, approaching the flow towards two-dimensional. Thus, the low value of A_B in conjunction with the high value of A_T can result in a very low critical angle for the flame acceleration.

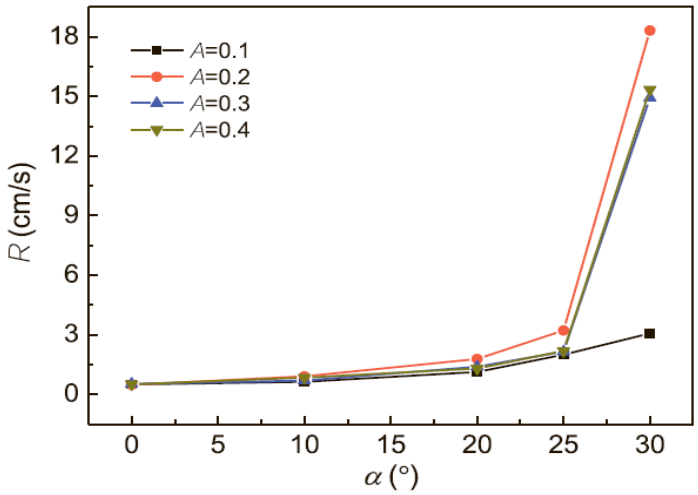

Figure 13. Rate of flame spread as a function of inclination angle [31]

Additionally, there are numerous studies that prove that the trench aspect ratio is an influential factor in the flame spread rate. Xie et al. [31] conducted several experiments with trenches to investigate eruptive fire behaviour in channel geometry. Figure 13 illustrates the flame spread rate as a function of the inclination angle of the trench. As can be seen, there is no significant change in flame spread rate up to 25° for all tested channel aspect ratios, so the fire spread is steady. However, the further increase of the slope leads to a dramatic change in the spread rate for aspect ratios more than 0.1. This region indicates that the fire spread becomes unsteady, i.e. this is an acceleration region where the heat transfer from the flame to an unburnt fuel is considerably enhanced. The authors concluded that aspect ratio has a little effect on the rate of flame spread until critical 30° for these experiments, but then the rate of flame spread greatly depends on the trench aspect ratio. An et al. [37] also concluded that trench aspect ratio is an influential parameter. The authors investigated the flame spread rate on a vertically oriented U-shaped façade and plotted a graph showing flame spread rate versus structure factor (same as trench aspect ratio) that can be seen in Fig. 14.

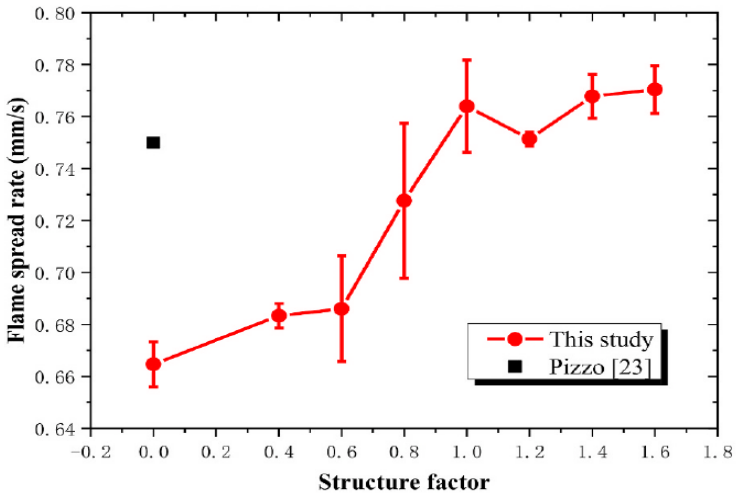

Figure 14. Flame spread rate as a function of trench aspect ratio [37]

An et al. considered a wide range of the trench aspect ratios to see the general trend. The results are consistent with previous studies that the stronger the restriction of lateral entrainment, the higher flame spread rate is expected. According to the article, the chimney effect will be intensified with an increase in the aspect ratio since the entrainment from the front side is weakened and the only possible way to entrain is a bottom part. This effect extends the flame height along with the burning material and increases preheating zone length, accelerating flame spread. Note that the flame spread rate in this experiment remains stable due to relatively short samples (30 cm), and as explained by the authors, the acceleration occurs only when the sample is long enough. According to Quintiere et al. [38] the size of the tested model shall be long enough to observe the turbulence flow that appears when the sample is longer than 0.3 m. Furthermore, it can be seen from the figure that for aspect ratios less than 1 flame spread rate increases with an increase of sidewalls, however after the "critical" value of 1, the spread rate remains relatively stable.

Another recent study by Chen et al. [7] was focused on the flame spread in an inclined trench that has different ratios between upper and lower volume that can be observed in Fig. 15. It should be noted that the plywood used in the study was ignited from two sides (from region A and region B) to investigate the influence of the ratio β. Region A is ventilation-controlled and region B is fuel-controlled.

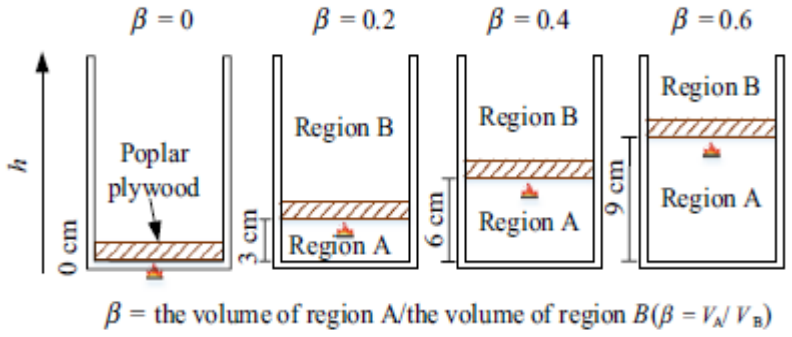

Figure 15. Volume ratios in a trench [7]

The main observation is consistent with the previous researches that the higher the inclination of the trench gives the faster the flame spread. Also, the authors found that plywood samples burn faster in the middle of the trench and burn faster at the top of the trench than in the bottom. Figure 16 shows the distribution of velocities along the 45° trench and estimates the influence of the volume ratio. The researchers divided the trench length into 5 regions depending on the flame spread rate, where the central acceleration region generates the highest rates due to additional preheating. As can be seen, the highest rate belongs to β=0.4, which means that volumes from top and bottom are almost equal, while for β=0.2 the rate has the lowest value probably due to a strong dependence on oxygen availability. Nevertheless, further investigation showed that each inclination corresponds to a certain critical β value, which gives maximum flame spread rate in the middle of the channel.

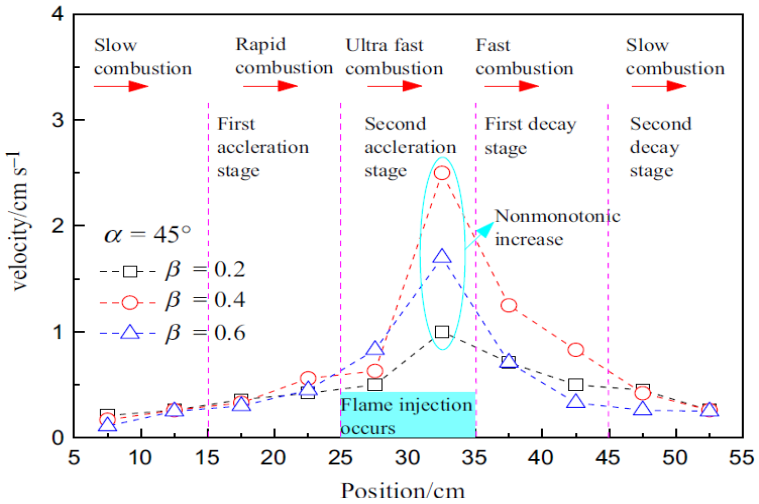

Figure 16. Flame spread rate [7]

Tsai et al. [39] focused on a topic of a width effect on a vertical flame spread rate in channel geometry. Remarkably, the behaviour of fire is different when sidewalls are

present. In general, both cases show the growth of the spread rate with an increase of the width since the influence of the lateral fuel diffusion is stronger and as consequence flames were higher. However, the relative change of the flame spread between trench and non-trench is not uniform. For the width range from 100 to 300 mm the flame spread rate was higher compared with the samples without sidewalls, because of the stronger heat feedback and higher flame height in a trench that ensures intensified preheating of the fuel. Yet at 500 mm the rates were almost identical and finally, at 700 mm the spread rate was higher for the non-trench sample. The authors explain that phenomenon by the improved mixing of the between pyrolyzate and the entrained air when the sidewalls were absent at wider samples that provides more efficient combustion and stronger heat feedback. This study result is consistent with Macmillan et al. [36], who reported that the trench effect was more pronounced when the channel was narrower. Referring to the above-mentioned literature, when the trench bed is narrower the aspect ratio will be higher and that means the flame spread will be also higher which is also consistent with Tsai and Macmillan's findings.

1.5 Energy balance in a trench

Based on the available literature it becomes possible to describe a heat transfer process and specify some distinctive features of the energy balance inside the trench. According to Fernandez-Pello et al. [16], the solution of the concurrent flame spread problem is concluded in solving a solid phase energy equation with the heat flux at the surface as a primary boundary condition. Also, they mentioned that normal temperature gradients are much larger than gradients along the surface, thus the one-dimensional transient form of energy equation will be enough to describe the heat transfer. Also, the contribution of streamwise conduction in the solid phase is comparably small, since the speed of the thermal wave through the solid is considerably lower than through the gas phase in the case of an upward flame spread [40]. Thus, one-dimensional Fourier field equation for unsteady state conduction inside the solid [41] is expressed in the following form:

$$\frac{\partial T}{\partial t} = \alpha \frac{\partial^2 T}{\partial x^2} \tag{6}$$

It should be specified that at the beginning of tests the temperature of the fuel is uniform and once it is heated by the external heat flux $\dot{q}''_{ig}$ the conduction into the solid takes place. The thickness of the material L in this work is not infinite, therefore the

boundary condition on the back side is expressed via convection and conduction. So, the boundary conditions are:

$$T(x) = T_0 \; t = 0 \tag{7}$$

$$-k\frac{\partial T}{\partial x}_{x=0} = \dot{q}^{"}_{ig}(x,t) \tag{8}$$

$$-k\frac{\partial T}{\partial x}_{x=L} = h(T_s - T_0) \tag{9}$$

To express the energy balance across the surface that is responsible for the ignition of the sold, it is better to describe it in a very simple form first. The heat that is sufficient for ignition of the solid surface is equal to heat flux coming from the flames minus the losses from that surface:

$$\dot{q}''_{fl} - \dot{q}''_{loss} = \dot{q}''_{ig} \tag{10}$$

It was shown previously that the dominant modes of heat transfer in a trench are radiation $\dot{q}^{"}_{rad}$ and convection $\dot{q}^{"}_{conv}$, where conduction through the gas phase can be omitted. The term $\dot{q}''_{fl}$ can be written in the following form:

$$\dot{q}''_{fl} = \dot{q}^{"}_{conv} + \dot{q}^{"}_{rad} \tag{11}$$

However, the heat losses should be described more extensively since the upward flame spread is not steady. According to Pizzo et al. [42] and Orloff et al. [43], transient burning of PMMA is accompanied by in-depth radiation and conduction that have to be taken into account in the surface energy balance. Figure 17 shows the schematic representation of heat transfer across the surface control volume.

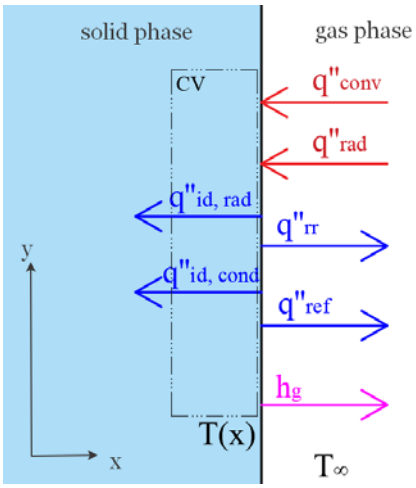

Figure 17. The schematic diagram for a heat transfer in a trench

From the figure, it can be observed that losses from the surface (blue arrows) in general constitutes of radiation and in-depth conduction that is written below:

$$\dot{q}''_{loss} = \dot{q}''_{rr} + \dot{q}''_{ref} + \dot{q}''_{id,rad} + \dot{q}''_{id,cond} \quad (12)$$

Thus, the full energy balance can be rewritten in the following form:

$$h(T_f - T_s) + (1 - \rho_r)\varepsilon_f \sigma T_f^4 F_{12} - \varepsilon_s \sigma T_s^4 - \dot{q}''_{id,cond} - \dot{q}''_{id,rad} = \dot{q}''_{ig} \quad (13)$$

In turn, the received heat is required to raise the temperature to its ignition value and also melt, vaporize and pyrolyze:

$$\dot{q}''_{ig} = \dot{m}'' h_g = \dot{m}'' \left(\int_{T_\infty}^{T_p} C dT + h_{melt} + h_{vap} + h_{pyr} \right) \quad (14)$$

This energy balance was devised for a surface with an upward concurrent flame spread, yet for the trench geometry, the terms appear to be the same. However, the order of magnitude will be considerably higher, since the sidewalls alter the interaction of heat and the surrounding environment. Referring to Yan et al. [9], when the sidewalls are mounted, they restrict the dissipation of the radiation and reflect it to the fuel surface. Furthermore, sidewalls are also heated during the flame spread, which means that the net radiation received by hot sidewalls will be lower than in the cold unrestricted environment due to smaller temperature differences. So, there is additional heat feedback that enhances flame spread. Moreover, a convective current, which in the case of unrestricted plume dissipates to the environment, flows inside the channel, extending preheating length and intensifying the heat transfer. Last but not least, when the fire is in a trench, the flame attachment is more pronounced, which means that view factor will be higher and the radiative term will be also higher.

1.6 Problem definition

The analyzed scope of the scientific works gives a clear picture that the trench effect phenomenon was extensively investigated during a relatively short period about 25 years ago. Without a doubt, some significant works were made recently and help to understand this effect better. However, some questions arise when it comes to explaining the behaviour of fire in a trench at steep angles less than 90°. For example, some fluctuating behaviour of the flame spread velocity was observed in the research work from Beswick et al. [44] who carried out some experiments with thermally thin material in trenches in

a range from horizontal to a vertical position. It was found that in the range from 45° to 70° the flame spread remains relatively stable, but after that rapidly rises again. On a contrary, the previous research by Drysdale et al. that was discussed above shows two main "elbows" from Figure 10. The first one is a well-explained trench effect at lower angles, and the second change is when the flame spread velocity comes back to a gradual rise after approximately 40°. The results from these studies contradict each other, showing ambiguity in flame spread research.

After the above discussion, it becomes clear that there are plenty of research studies that focus on the determination of the critical angle and flame behaviour in a trench at lower angles of inclination. It seems to be necessary to do a thorough investigation of the trench effect at angles higher than 45 degrees to fully understand and predict the behaviour of fire in such geometries and finally answer the question "Is there a vertical trench effect"?

1.7 Aim and Objectives

The main aim of this thesis is to experimentally investigate the flame spread along the trench geometry, particularly the flame propagation at the angles between 50 and 90 degrees. The research can contribute to a better understanding of the flame behaviour in the steeply inclined channels that can be taken into account in some fire safety applications in the future. During this study, some distinctive features of the flame spread in the trench were revealed.

The main objectives of this work are:

1. Observe and describe a flame spread pattern in a trench at different steep angles;
2. Quantify and compare flame spread rates at tested angles with and without sidewalls;
3. Investigate the potential influence of a trench aspect ratio on a flame spread at steep angles.

Chapter 2 Methodology

2.1 Materials

The material that was used throughout the work is PMMA (Polymethylmethacrylate) which is known as "bench mark material" since it is a well-known and widely applied material in experimental fire studies [45]. First of all, PMMA is relatively cheap and available in a local market, so there is no difficulty to carry out a big number of tests if needed. Also, it is possible to choose the desired thickness of the material and easily cut a sheet into smaller pieces. It is a relatively lightweight and non-charring material that forms fine bubbles when heated and softened. In contrast, charring materials produce a substantial amount of unknown parameters that complicate the further detailed analysis of a flame spread problem [16]. So, all these characteristics are suitable for this study to easily observe the propagation of a pyrolysis front.

In order to choose the thickness of a PMMA sample, it is necessary to determine the expected regime of the heat transfer within a solid. There are two main regimes that depend on the solid thickness namely, thermally thick and thermally thin. Thermally thin behaviour is frequently characterized by two-sided burning because of a very small temperature gradient in the material. Gas phase becomes the main heat transfer mechanism in this case and the spread rate becomes proportional to the thickness [45]. When the material becomes thicker, the role of the heat transfer through the solid media is more substantial due to the increased importance of conduction and the presence of a strong thermal gradient [46], where thermal penetration depth $\delta < t$ is smaller than thickness of the material. For sufficiently thick fuels the temperature distribution does not change across the thickness and the flame spread rate becomes independent of the fuel thickness [45]. However, it was found that at steep angles heat transfer to the sample occurs primarily through the gas phase, so the contribution of conduction through the solid phase to the unburnt fuel is negligibly small since the time for a thermal wave to propagate through the sample thickness is small compared with a rate of flame spread [40].

Ito et al. [40] found that thermal penetration depth δ is nearly independent of the sample orientation, so it mainly depends on the material characteristics. This parameter can be calculated by the following formula:

$$\delta = \sqrt{\alpha\tau} \quad (15)$$

From the experiments from that study, the thermal penetration depth for a PMMA sample was equal to approximately 2.2 mm. Quintiere [23] also mentioned that heating depth is dependent on heat flux and generally for most of flame spread heat fluxes the approximated value between thermally thick and thin behaviour is 2 mm. Furthermore, Hirano et al. [45] observed that for the thicknesses between 2 mm and 2 cm both gas and solid-phase become important. For this thesis work it was arranged to use the sample thicknesses 10 mm and 20 mm that can be considered as a thermally thick fuel. To prevent the burnout stage at lower angles of inclination, 20 mm samples were used for angles lower than 30°.

Furthermore, the flame spread over the thick fuels is inherently non-steady (acceleratory) [47], since the pyrolysis length x_p increases in time. Hence, thick materials might be even more hazardous in a trench, so the usage of thick PMMA is more relevant for this study from the fire safety point of view. According to Drysdale's findings [32], a steady state will not be reached until a constant burning area x_p establishes, the length of which depends on the burnout time of the fuel. Apparently, this time depends on the fuel thickness, so the thicker the fuel the more severe upward flame spread is expected.

The width of PMMA was chosen to be uniform for all experiments in order to decrease the number of variables in sample size and as a consequence the overall number of tests. Besides the geometrical variables, it was decided to use two types of PMMA – clear and black to see the possible impact of a material emissivity on the surface flame spread. The overall sample configuration for the tests can be found in Table 2 below.

Table 2. Sample configuration

	Length, mm	Width, mm	Thickness, mm	Colour
Configuration A	500	100	10	Clear
Configuration B	500	100	10	Black
Configuration C	500	100	20	Clear

Vermiculite boards will be used as sidewalls in these experiments. This material has good thermal insulation characteristics and that helps to keep the convective and radiative heat inside the channel, revealing the trench effect. As was mentioned before, the trench aspect ratio A_T has a major influence on the flame spread rate, thus for this work, three sizes of vermiculite boards were determined which can be seen in Table 3

below. Also, in this work A_T is denoted as A in the discussion part for simplicity since there is only aspect ratio parameter that was varied.

Table 3. Vermiculite boards dimensions

Trench ratio A=H/W	Length, mm	Width, mm	Thickness, mm
0.5	500	50	20
1	500	100	20
1.5	500	150	20

2.2 Experimental set-up

The main aim of this experimental work is to measure the propagation of the pyrolysis front and capture some distinctive features of the flame spread in the trench geometry and compare it with samples without sidewalls. To measure this, two different methods were used, namely the video recording method and temperature measurement by thermocouples. The overview of the experimental setup can be seen in Fig. 18.

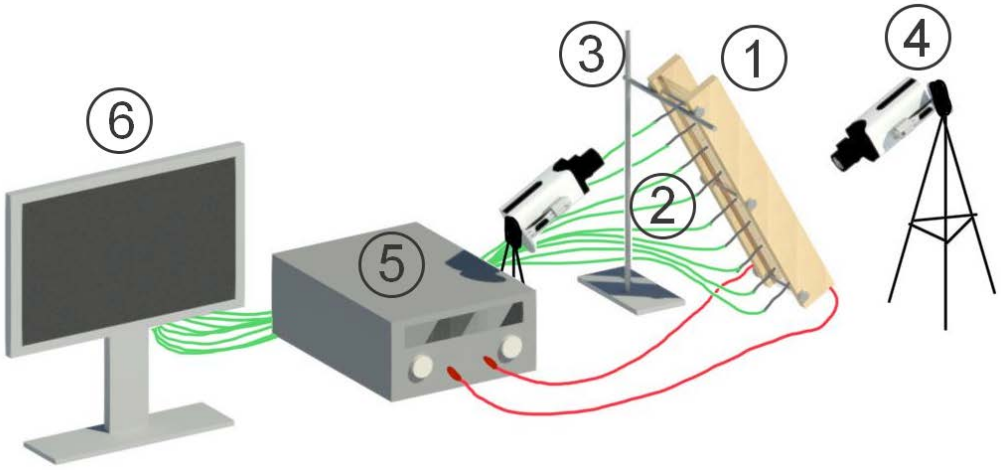

Figure 18. The experimental set-up, where (1) Trench sample, (2) 9 thermocouples, (3) steel holder, (4) two video cameras, (5) power supply, (6) data logger + computer

Each trench sample (1) is made of two vermiculite boards that tightly clamp the PMMA slab with three stainless nuts and washers. This assembly allows to vary the height of sidewalls easily, without additional consumption of vermiculite material. Figure 19 (a-c) shows two types of PMMA material used in the work and how the slab is incorporated into the trench. It was decided to mark both black and clear slabs with 9 lines at a distance of 5 cm from each other which will help to track the pyrolysis front location. However, the first line was set at 70 mm from the bottom edge of the sample for convenience during the test. Apart from that, Fig. 19 (d) depicts the configuration without sidewalls that can be made with the rear side of the same trench, clamping the slab at the level of the rear

sidewall edge. This arrangement helps to avoid three-dimensional edge burning of the PMMA slab and focus only on the upward flame spread.

Figure 19. Trench components. (a) Black and clear PMMA samples, (b) trench bottom view, (c) trench front view, (d) trench arrangement for samples without sidewalls

The metal holder (3) from Fig. 18 was chosen to simply support the trench when it is inclined since the height can be adjusted easily with a one fixing screw. Also, there are two cameras (4) used in the experiments to track the propagation of the pyrolysis and flame front from both sides, namely iPhone XR with 60 fps for the rear side and Panasonic HC-V380 for the front side. It is crucial to record videos from both sides for consistency of the results since in the case of black opaque PMMA the only possible way to observe the pyrolysis front is the front side, while for clear PMMA the most convenient side for observation is the back. Additionally, the advancement of the flame front can be only tracked from the front that makes the usage of two video cameras quite relevant.

The slab was ignited by applying current through a fixed wire that heats up and then ignites the PMMA. The Nichrome (80% Ni +20% Cr) wire is fixed by two ceramic screw terminal blocks on each side of the walls. Figure 20 (a-b) demonstrates the pre-ignition and post-ignition state in the trench with the applied wire. The protected cable from the power supply device is connected from the other side of the box, creating an enclosed circuit. Skytronic 650.682 power supply produces 9.5 A and 6.6 V during the test that is shown in Fig. 20 (c). Unlike the piloted ignition, this method allows to ignite the sample simultaneously across the whole width and ensure sustained flaming of the fuel in a

relatively short time. Also, a foil tape was used at the bottom face of the slab to prevent the propagation of the flames in the downward direction (see Fig. 20 d).

Figure 20. Ignition set up. (a) wire before the ignition (b) wire at the beginning of the test (c) power supply parameters (d) foil protection of the bottom part

Nine K-type thermocouples d=1 mm in diameter were embedded to the rear side of the sample to measure the temperature change in the solid phase. Figure 21 shows the layout of the thermocouple location from TC1 to TC9. It can be seen that the position of each thermocouple corresponds to the marked line for a pyrolysis front tracking, that is convenient for matching the data during the post-processing stage. It should be noted that the holes for thermocouple wires were drilled not through the whole thickness of the PMMA; 1 mm of the material was left between the thermocouple and the surface. It was done mainly for two reasons. Firstly, it was easier to fix the thermocouple when it is cramped inside the material and secondly, the main intention was to measure the temperature in the solid phase of the material.

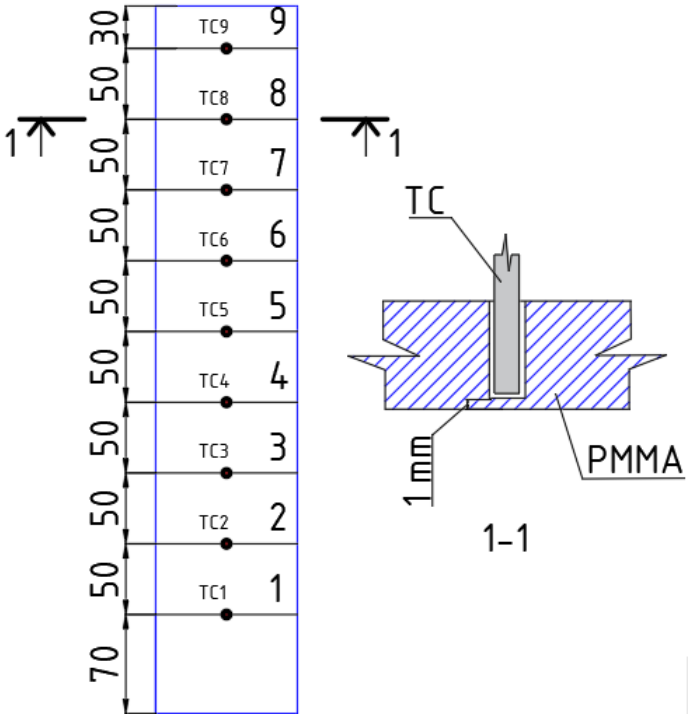

Figure 21. Sketch of thermocouple arrangement and its penetration depth

In order to record the temperature change, a data logger was used that can log the temperature data every one second during each test.

2.3 Experimental procedure

Three sample inclinations were initially chosen to observe the flame spread at steep angles, namely 50°,70° and 90° degrees. After that, lower angles were also tested for further comparison in this work. Figure 22 shows the visualization of the inclined trenches and the reference point for tilting before the start of the test.

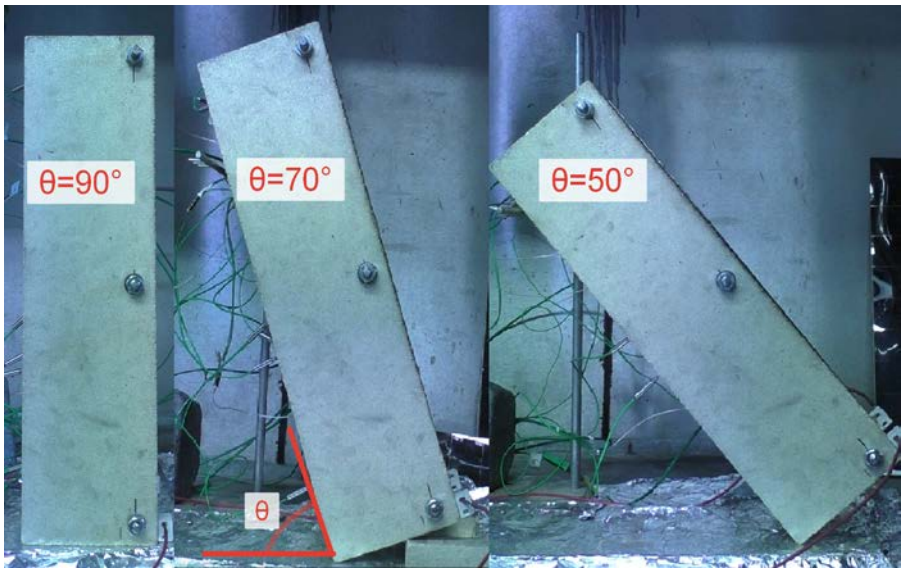

Figure 22. Inclination angles

Twenty-three (23) trials were conducted in total using different experimental configurations. A single trial was conducted for each configuration tested. The full experimental matrix can be observed in Table 4 below.

Table 4. Experimental matrix

Test Number	Angle °	Configuration*	Aspect ratio, H/W
1	90	A	1
2	70	A	1
3	50	A	1
4	90	A	N/A
5	70	A	N/A
6	50	A	N/A
7	90	B	1
8	70	B	1
9	50	B	1
10	90	B	N/A
11	70	B	N/A
12	50	B	N/A
13	90	A	0.5
14	70	A	0.5
15	50	A	0.5
16	90	B	1.5
17	70	B	1.5
18	50	B	1.5
19	15	C	1
20	30	C	1
21	23	C	1
22	23	C	N/A
23	15	C	N/A
Additional tests			
1a	90	A	1
7a	90	B	1

* - See Table 2 for details

The video recording method is the main source of data for these experiments since the pyrolysis front was tracked based on a revision of the recorded video materials and this method seems to be more reliable and convenient for an observer. Temperature measurements in this work play only a supplementary role for an additional analysis after the main discussion based on video data results.

As was mentioned before, PMMA can produce a fine distinctive bubbling front when it is heated that can be a reference point for the flame spread measurements. The resolution of a video camera has to be sufficiently high to observe the detailed propagation of the bubbling front. For instance, Fig. 23 depicts the sequence of images

from the test with a vertically oriented clear trench, where white lines indicate the shape and height x_p of the pyrolysis front measured on the rear side of the trench.

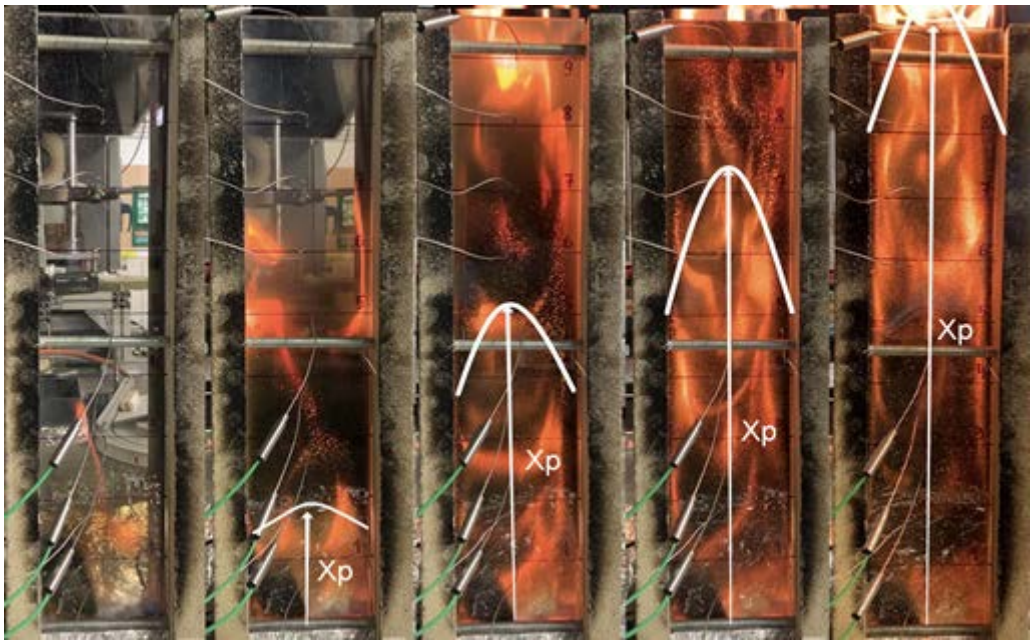

Figure 23. Example of the pyrolysis front propagation

In general, the testing procedure consists of three main stages: ignition, burning, and suppression. During the ignition stage, the hot wire transfers a sufficient amount of heat towards the PMMA sample via conduction. The heating process occurs until sustain flaming on the fuel surface is established and the bubbling front starts to move upward (approximately 60-90 seconds), only then the wire is switched off. The first control line on the sample is arranged to be the starting point for the flame spread data recordings. The data logged below the first line (first 70 mm) are not taken into account since the pyrolysis front is not stable and pronounced in this region. Besides, the heating time of the slab is not a fixed value, it changes from test to test, producing different velocities at the beginning of the experiment. In addition, series of thermocouples record the temperature change along the slab for further comparison with the data from visual observation.

As soon as the pyrolysis front reaches the top and bubbles appear on the top edge surface, the experiment is finished. The last stage is fire suppression by applying water spray on the burning surface.

Chapter 3 Experimental results and discussion

3.1 Qualitative experimental observations

After series of experiments, it became possible to observe the general trend of the flame spread with and without sidewalls. However, the sidewalls used in the experiments are not transparent, so it impossible to observe some changes in the flame behaviour from the side view when the sidewalls are mounted. In order to compare the flame extension both for the trench and no trench geometry, the front pyrolyzing side was used for the investigation. Also, Fig. 24 shows the main terms that will be used to describe the dimensions of the flame during the concurrent mode of flame spread.

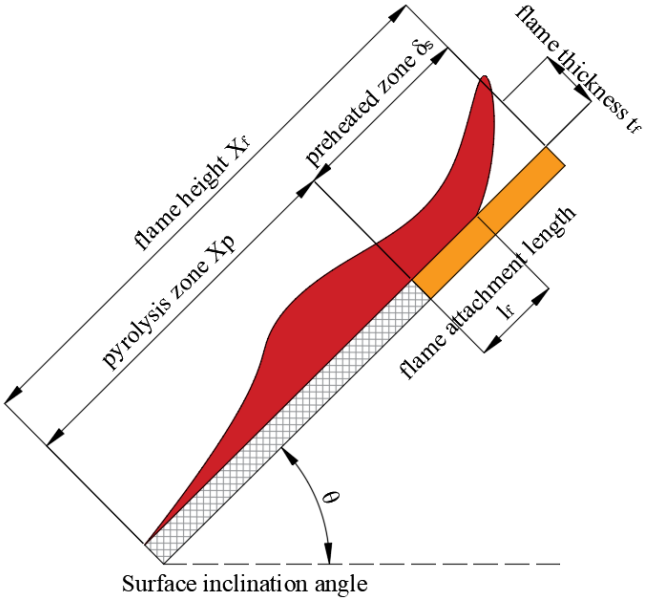

Figure 24. Flame geometry definition

Figure 25 shows the sequence of snapshots made for three angles with four variable aspect ratios, twelve pictures in total. It should be noted that images were taken at the moment when the pyrolysis front has reached line number 4 (220 mm). This suggests that the burning area is equal in each case that allows obtaining consistent and comparable graphical data.

As can be seen, the flame height x_f varies a lot even within a single value of the angle. For example, when the sample is inclined at 50 degrees, the flame height for aspect ratio = 0 (no sidewalls) is much lower than for the cases with sidewalls. The difference can be explained based on the revised scope of the literature review. The Coanda effect and restricted entrainment of air from the sides play a considerable role in the flame elongation when the flame is in the channel.

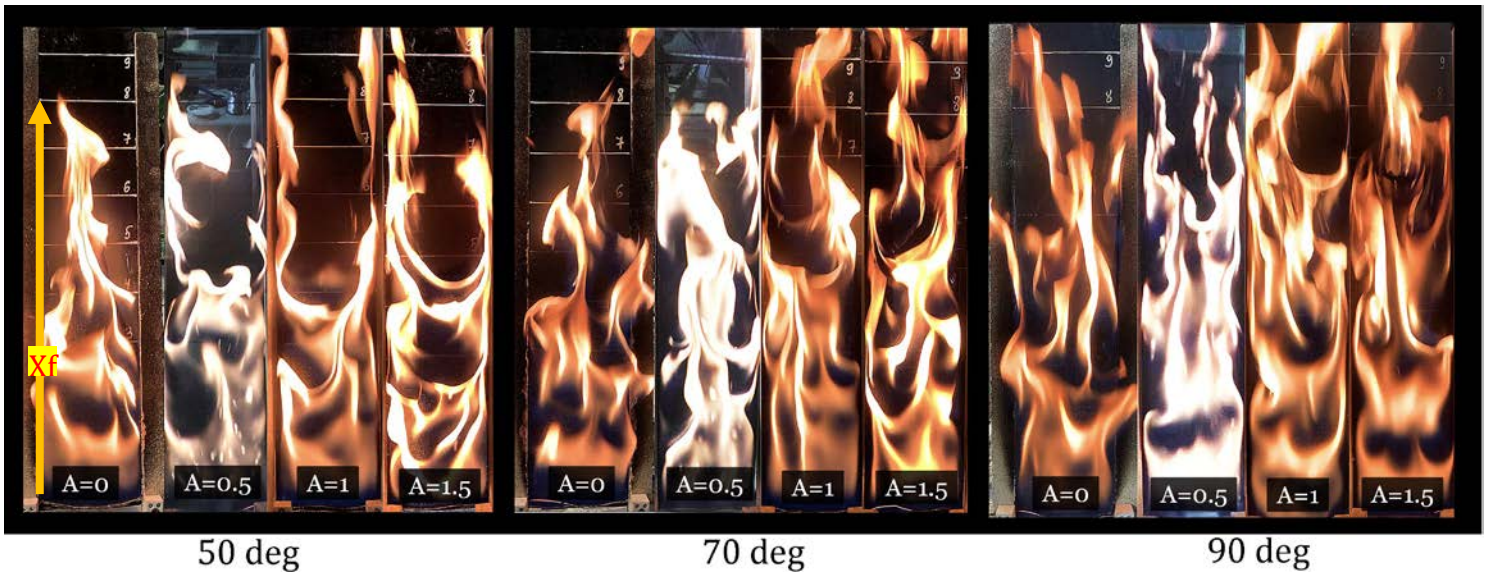

Figure 25. Flame length observation at angles 50, 70, 90

Apart from this observation, the data are consistent with the previously mentioned work, where the difference in the flame height between two types of samples was described analytically by Saito et al. [21] by the following expression:

$$x_f = K\left[\dot{Q}' + q\int_0^{x_p} \dot{m}''\,dx\right]^n \tag{16}$$

Where,

n – constant,

K —constant, that K = 1 for open walls and K = 1.25 for walls protected with sidewalls.

When the sidewalls are installed, the applied factor K = 1.25 is higher for the case with restricted entrainment that leads to the bigger value of the flame height. However, this formula is applicable only for a rough estimation of the flame length between the trench and no trench geometry, since it cannot facilitate the understanding of the difference of the flame length between different aspect ratios. Also, from Figure 25 it can be seen that the flame height becomes slightly bigger with an increase of the height of the sidewalls within one value of the inclination angle. This can be explained by the stronger influence of the channeling effect since with the increase of the sidewalls the only possible way to entrain air is the top and bottom parts of the trench. Furthermore, as the angle increases the flame height becomes also bigger, reaching the maximum flame extension at 90 degrees. Since the video camera was inclined to be parallel to the burning surface, it was impossible to capture the flame thickness, so the flame height term is not sufficient

to describe the changes when the trench orientation is varied. Flame attachment length should be additionally used to explain the difference in the flame height between 50-70-90 degrees. When the sample is vertically oriented, the flame attachment length reaching the maximum value among the range of the tested samples. At 50 degrees the flame tip deviates from the surface plane, going in the perpendicular direction to the camera view. This change in the flame attachment can be explained by the sequence of screenshots on flat samples in Fig. 26.

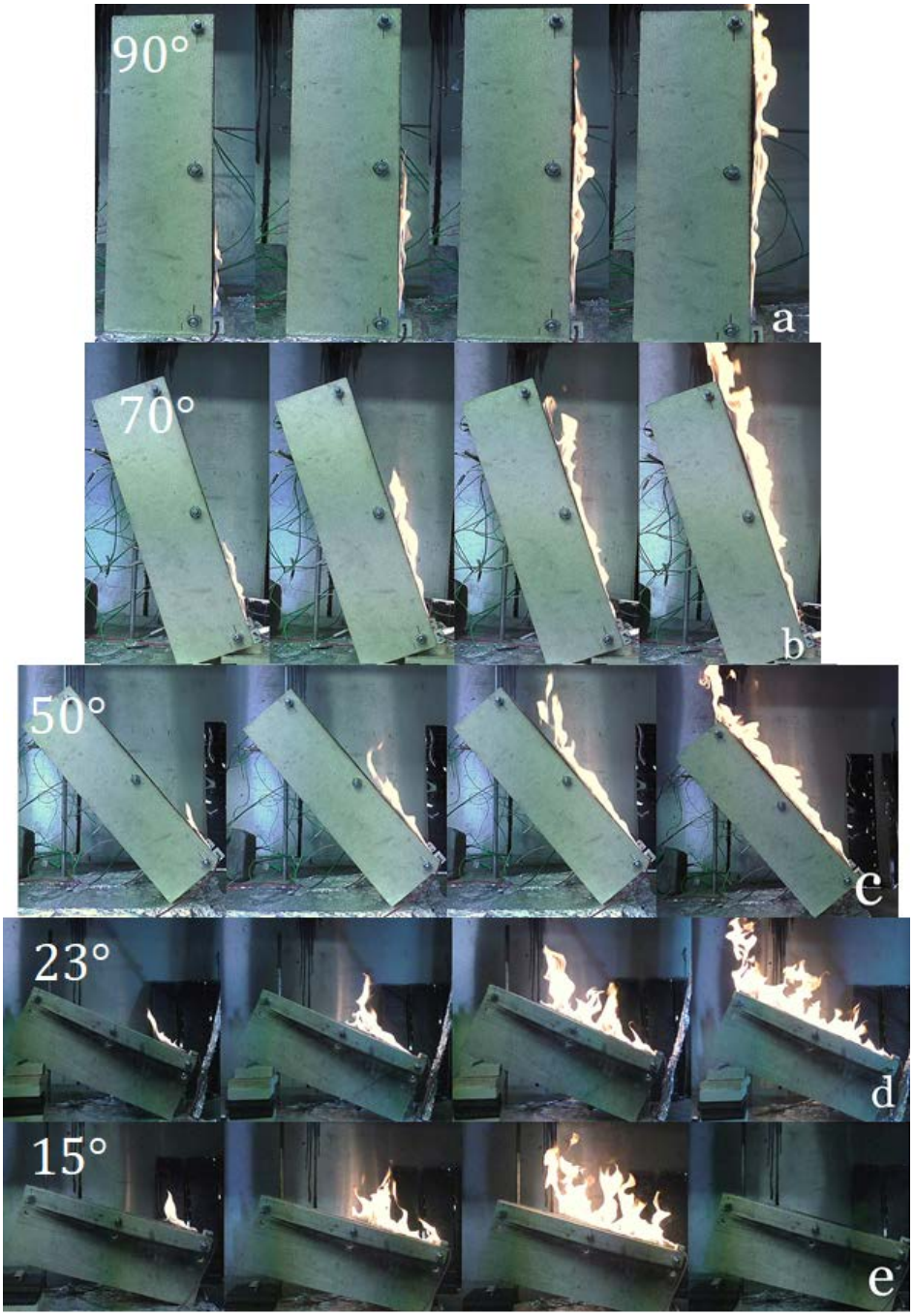

Figure 26. Flame behaviour at different angles when flame front reaches 25%, 50%, 75% and 100% of the sample length

The images were taken from the experiments with the samples without sidewalls in order to see the sides of the installation. At 90 degrees the flame is fully attached to the PMMA sample extending along the whole surface of the PMMA sample, thereby enhancing the heat transfer from the flame to the bigger area of the virgin material. While at 70 degrees it becomes possible to observe the flame tip that is slightly tilted towards the vertical plane, at 50 degrees this effect is more pronounced, but still pretty well-attached to the inclined surface. As was mentioned in the literature review, the flame spread rate is directly dependent on the preheated area by the tilted flames. The stronger the flame attachment, the faster ignition of the surface is expected to be. Additionally, a dramatic change in the flame attachment can be observed at 15 and 23 degrees, where the flames are purely buoyancy-dominated and do not have any tilting towards the surface. This trend can also be applied to the flame spread in the trench geometry but the value for a critical angle, at which the flame attachment occurs, will be lower judging by the Drysdale et al. [26] previously mentioned findings.

Another observation was made with the fire plume shape at the top of the trench and no trench sample that is shown in Figure 27 (a-d). From the video files it was found that at the moment when the pyrolysis front reaches the top point of the sample, the flame shape looks different for the trench and no trench geometry.

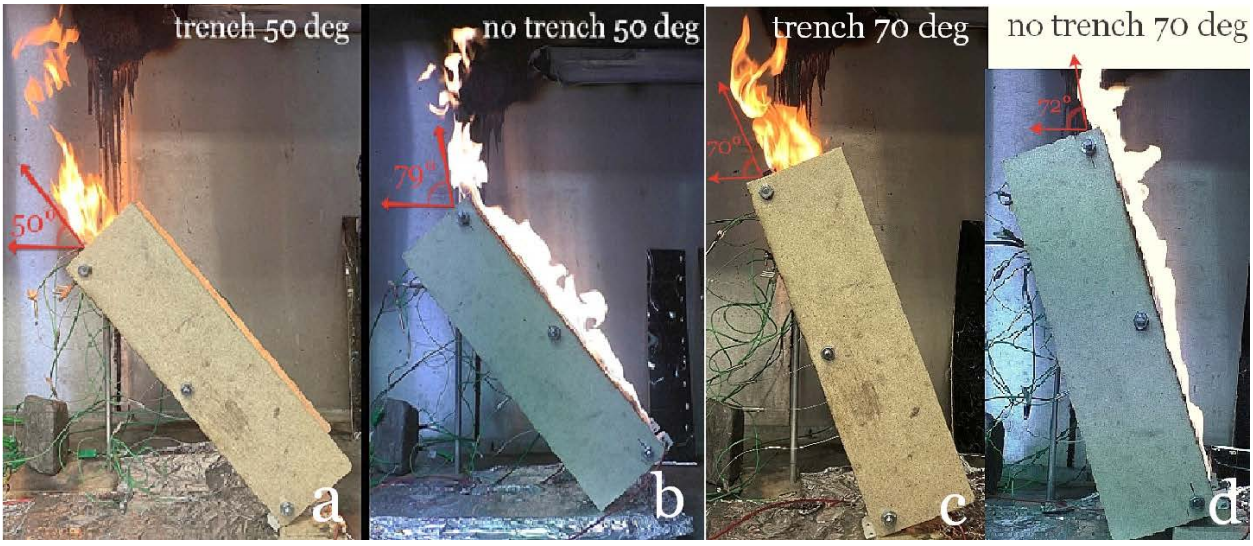

Figure 27 (a-d). The difference in the flame shape at the top of the sample

This distinction is more visible at 50 degrees, where the flame at the top of the trench resembles a jet flame compared with the sample with no sidewalls. The latter resembles a plume from the natural fire with lower velocity (lower Froude number).

According to Drysdale [14] the influence of momentum and buoyancy on a fire plume can be described by Froude number that is expressed below in a mathematical form:

$$Fr = U^2/gD \quad (17)$$

Also, the enhanced channeling effect may play the role in the shape of the fire plume. The more air entrained from the bottom, the stronger the channeling effect inside the trench will be, compared with the flame spread on an unrestricted surface. It means that the flames will have higher momentum (higher Froude number) on the exit of the trench that finally gives the different picture at the top. Furthermore, there is an inherent nature of fire to curve towards the centerline in the trench geometry to form a jet-like structure in the end [30], which also contributes to the specific shape at the top of the trench sample. Figure 28 proves the existence of this phenomenon in this series of experiments where the curved lines are indicated with blue arrows at the top of the trench.

Figure 28. Flames curving towards the centreline at the top of the trench

In general, the above-mentioned "jet effect" can be observed in all tested trenches that were steeper than 23 degrees, however, the deflection of the flame tip was different with an increase of the angle when the sidewalls were absent. For instance, at 50 degrees (Fig. 27a) the flames are well-attached to the PMMA surface in the channel and the flame tilting angle corresponds to the initial value of 50°. But for the sample with no sidewalls (Fig. 27b) the flame tip is deflected by 29° towards the vertical plane from the original 50° angle. Judging by the next pictures (Fig 27 c-d), it is clear that the deflection and the

difference between the flame from a trench and flat sample become smaller with an increase in the sample inclination. While Figure 27 (d) shows that the deflection of the fire plume is very small, Fig. 29 depicts no difference in flame tilting between two vertical configurations. The fire plume in the case of the vertically oriented samples looks very similar, except for the flame length that is still slightly higher for the trench geometry.

Figure 29. Vertically oriented samples

Another interesting observation was made at distinctive burning regimes along with the PMMA slab even at lower angles than vertical orientation. According to the Orloff et al. study devoted to vertical wall fires [43], approximately the first 10 cm of the slab has a laminar regime of burning that is characterized by smooth and thin flames where convection is a dominant mode of heat transfer (see Fig. 30). After this region, the behaviour of the flames changes considerably towards a turbulent regime with highly oscillating, radiative flames. It can be seen from the figure, that the length of the laminar region remains relatively constant across the 50°-90° range both for trenches (A=1) and flat samples.

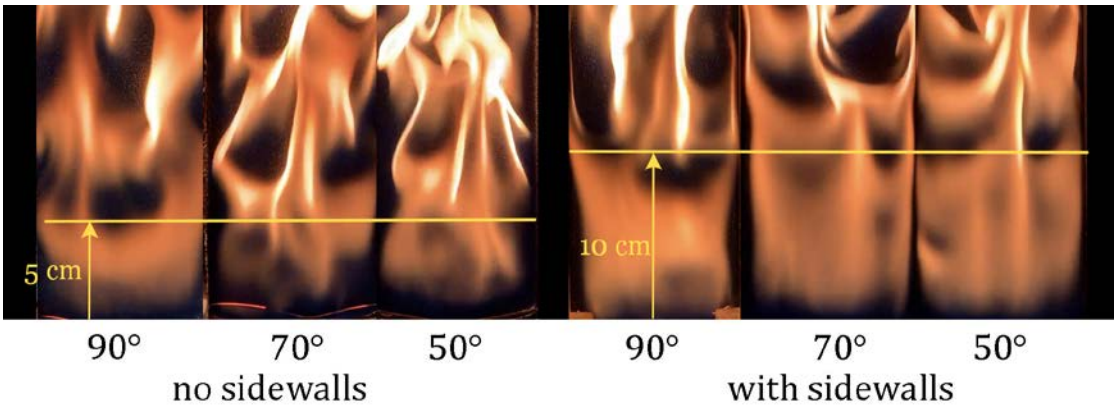

Figure 30. Laminar and turbulent regions along the burning surface

Nevertheless, the length of the laminar region was almost twice times bigger in a trench than in a flat sample. This phenomenon can be also induced by the enhanced channeling effect inside the trench and consequently increased velocities when sidewalls are installed. According to Drysdale's work [14], a buoyant fire plume (with low Fr) from natural fires is sensitive to external influence, so the increased air movement due to the chimney effect could affect the extension of the laminar flame region inside the trench.

Apart from the flame shape observation, the pattern of the pyrolysis front should be investigated in more detail as well. Figure 31 shows the pyrolysis and flame front shape on the samples without sidewalls from the front and back sides at 50-70-90° angles. It should be noted that the position of the pyrolysis and flame front is not captured at the same time in Fig. 31, because the main aim of this section is to discuss the shapes that were observed consistently throughout the test.

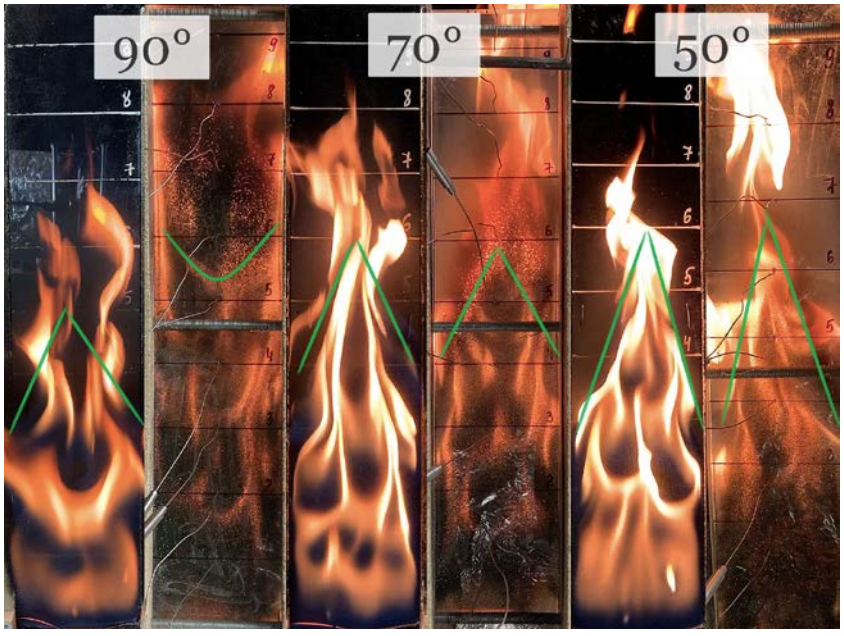

Figure 31. Pyrolysis front shape (no sidewalls)

It can be seen that the shapes of the pyrolysis and flame front can be different and vary with the angle of inclination. The most pronounced pyrolysis and the flame front were captured at 50 degrees where both fronts have a similar pointed triangular shape. However, at higher angles, the triangular shape becomes less pronounced and when the sample was installed vertically, the contour of the pyrolysis front finally switched to the U-shaped form. Notably, that in the vertical position the flame and pyrolysis shape does not correspond to each other, since the flame front still resembles a triangular contour and the pyrolysis front has the reversed trend. One of the possible reasons for such behaviour is that at lower angles the flame is not perfectly attached to the surface forming a partly free plume, as was shown in Fig. 26 (c). A free buoyant fire plume is subjected to a stronger influence of the side air entrainment that forms this triangular shape which can be observed in an unrestricted simple fire depicted in Fig. 32. Thus, the air entrainment hinders the propagation of the pyrolysis front on the sides and facilitates along the centerline, by pushing the pyrolyzate from the sides to the center.

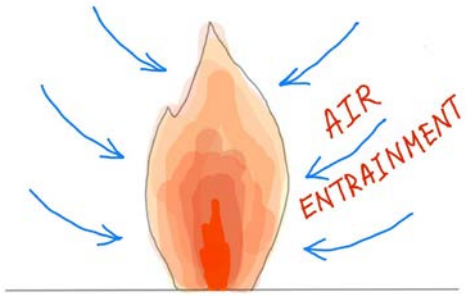

Figure 32. Influence of the air entrainment

The closer the angle to the 90-degree value the more attached the flame and less sharp the pyrolysis front was. As a result, when the sample is oriented vertically the propagation of the pyrolysis front at the edges is more pronounced due to the presence of side-edge burning phenomenon that was observed during all experiments without sidewalls. Although the PMMA slabs were clamped by vermiculite boards from the sides, the perfect alignment between materials was not ensured due to the crumbling nature of the clamping material. In this case, the uncovered edges represented a thermally thin material with an intensified heat transfer on both sides that finally gives a different contour of the pyrolysis front that is shown in Fig. 33 in more detail.

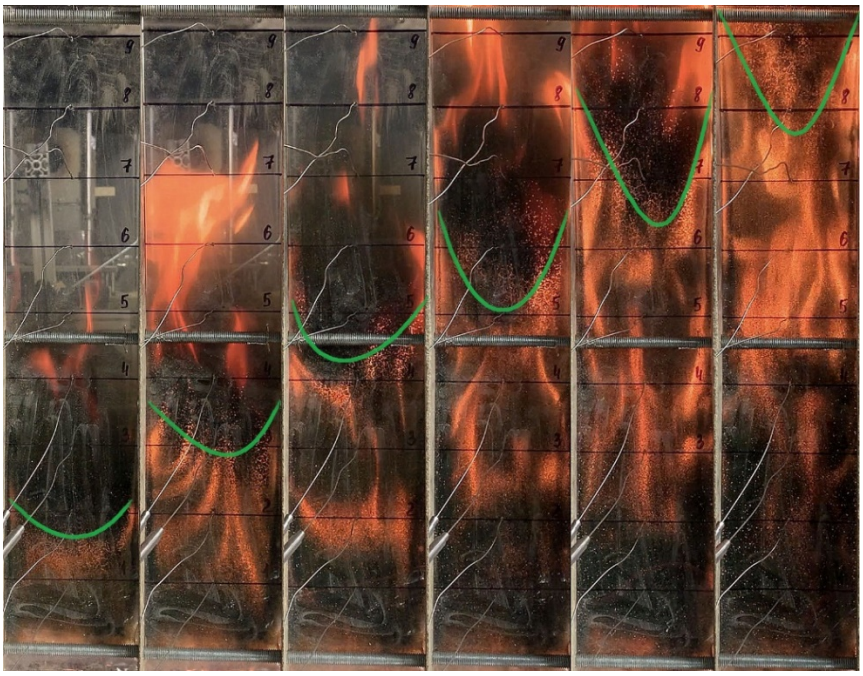

Figure 33. Propagation of the edge effect at 90 degrees

In contrast, a more uniform trend can be observed with the trench samples that are depicted in Fig. 34. The flame and pyrolysis front shape does not vary considerably throughout the tested range of angles, however in general the pyrolysis and flame contours in a trench are completely different from the contours of the flat samples. Firstly, the flame front has a distinctive U-shaped structure that can be observed in all trench samples.

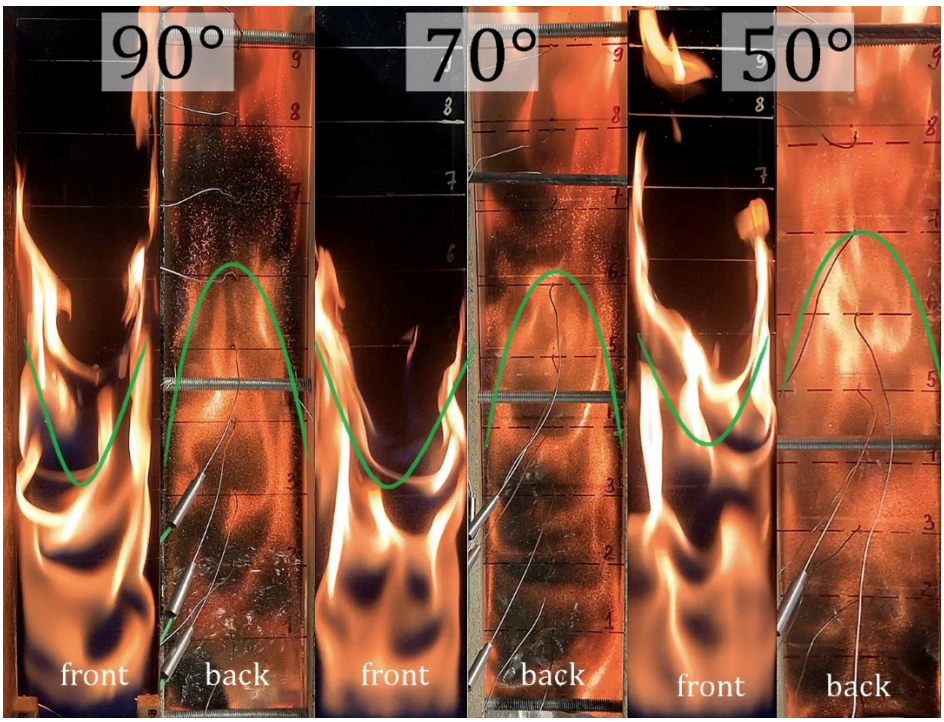

Figure 34. Pyrolysis front shape (with sidewalls)

This shape was formed due to the presence of sidewalls that prevents lateral entrainment. The pyrolyzate, which is produced at the sides, cannot diffuse in a lateral direction, thus it moves along the length of the trench inducing the significant extension near the edges. Also, the restricted air entrainment induces less mixing between the fuel and oxygen that probably makes a fire under-ventilated. According to Williams [12], when the fire is in an under-ventilated duct, flames tend to extend along the walls of the duct, not of the centerline that is shown in Fig. 35 below.

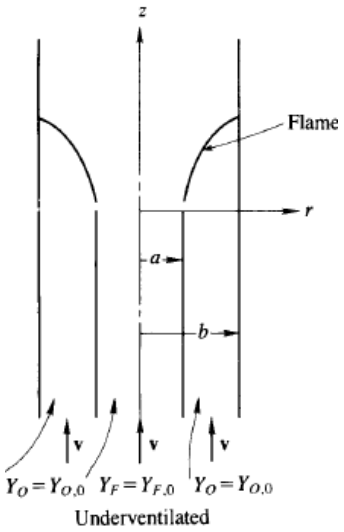

Figure 35. Flame extension in an under-ventilated duct [12]

Moreover, the Coanda effect inside the trench is responsible for a noticeable flame attachment to the surface of the sidewalls, creating a completely different picture in comparison with the samples without sidewalls that were discussed above.

Surprisingly, that the backside of the trench samples shows a quite different contour of the pyrolysis front that has an inverted U-shape. The reason for such discrepancy between the shape of flame and pyrolysis front might be a considerable heat loss from the PMMA slab to the vermiculite sidewalls that slows down a pyrolysis process at the sides of the sample. The consequences of such different flame spread patterns can be also investigated in Fig. 36 (a-c), where cross-sections of the trench and no trench samples are collected for comparison. The photos were taken after experiments with 50-degree samples, however, this burnout pattern was observed in all tested samples. Figure 36 (a-b) depicts the cross-section of the trench sample and the side part after the experiment. It is clear that the edges of the slab remained almost untouched by the pyrolysis process, while the burnout of the central part seems to be considerable. On a contrary, Fig. 36 (c)

reveals the effect of the edge burning, since the sides of the slab have significant burnout as well as the central part.

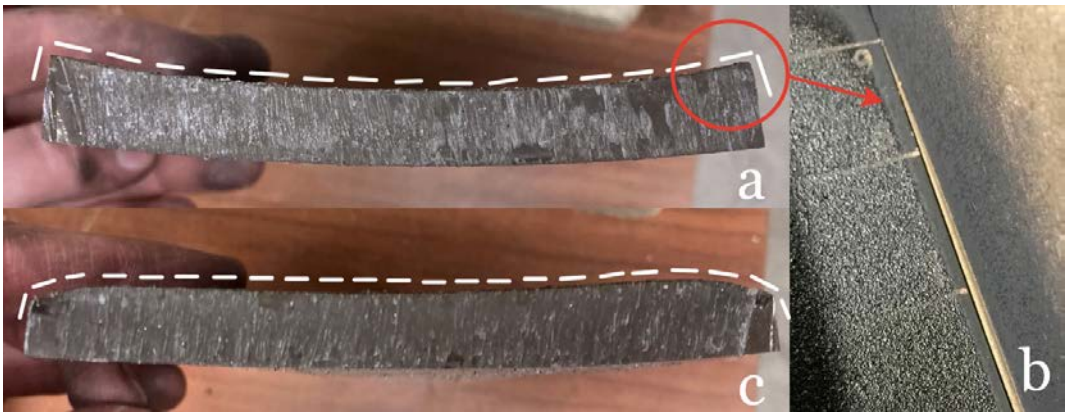

Figure 36. The shape of the samples after the experiment: (a) cross-section of the sidewall sample (b) virgin sides of the trench slab (c) cross-section of the flat sample

3.2 Pyrolysis front propagation

After thorough manual processing of the experimental video data, it became possible to plot the graphs of the pyrolysis front as a function of time that can be seen in Fig. 37. While the pyrolysis front data was observed to be fairly smooth and easily interpreted, the experimental data were fitted to an exponential curve for further analysis. Referring to Orloff et al. [43] the data were also quite accurately fitted to the exponential curves for reproducibility especially in the region after 20 cm, where a turbulent regime is developed. In this work, the approximation reliability value R^2 is relatively high for exponential fitting that was varied from R^2=0.9348 to 0.9972. Values of all data points can be also found in Appendix I.

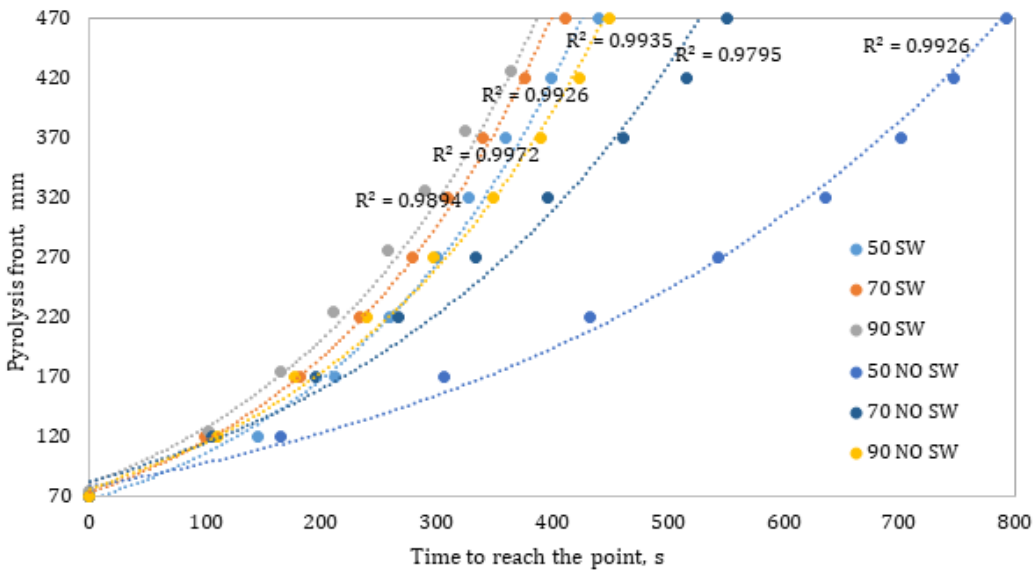

Figure 37. Pyrolysis front propagation and its exponential approximation

All graphs were fitted according to the following exponential law:

$$x_p = A \cdot e^{B \cdot t} \tag{18}$$

Where A *and* B – constants that can be seen in more detail in Appendix II

After all adjustments, Fig. 38 depicts the approximated graphs from all tested clear PMMA samples. Solid lines represent the propagation of the pyrolysis front in time inside the trench with an aspect ratio A=1. Dashed lines show the results for specimens without sidewalls ranged from 15 to 90 degrees.

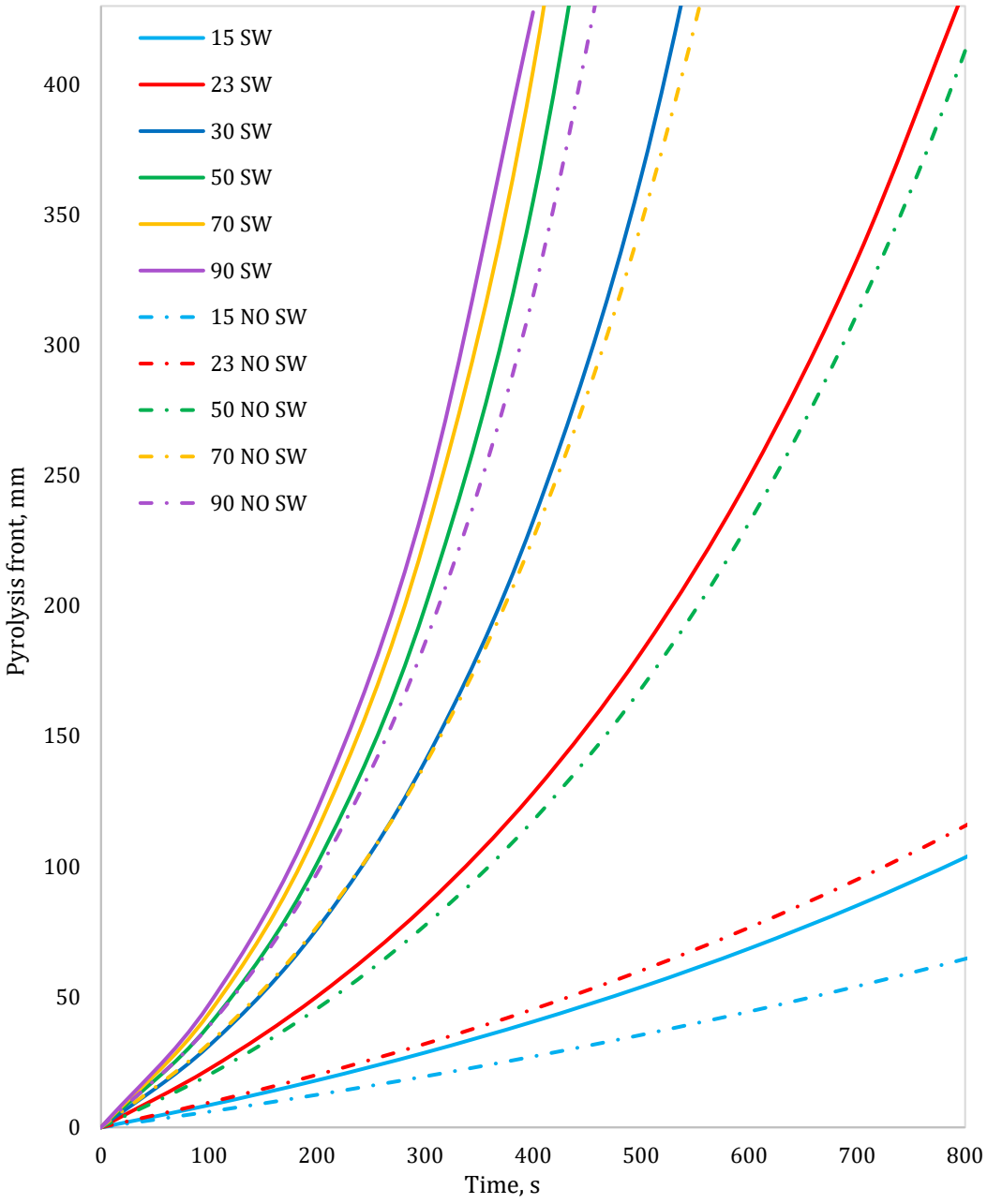

Figure 38. Pyrolysis front propagation of all tested angles

The overall picture is consistent with the previously reviewed literature where the samples inclined at higher angles produce faster flame spread and vice versa. Nonetheless, this trend does not have a gradual change for the samples with sidewalls. For example, the trench graphs, denoted as “SW”, are located very close to each other at 50-70-90 degrees. It means that the propagation of the pyrolysis front at these angles has a very similar intensity. However, the divergence between 15 and 23-degree SW-graphs is quite large compared with the results from the higher angles. In contrast, flat samples denoted “NO SW” show a more gradual increase in the pyrolysis front propagation without such rapid discrepancies. In addition, the progression of the pyrolysis front in the trench is always faster than in the corresponding flat PMMA samples, however, the difference between the lines varies considerably.

Figure 39 (a-e) depicts how the difference between pyrolysis front graphs varies with an increase of the inclination angle. Each graph represents the pyrolysis front evolution in time for both trench and no trench samples at a certain angle. Moreover, it was decided to measure the pyrolysis front location several times to obtain the error bars shown in the figures below.

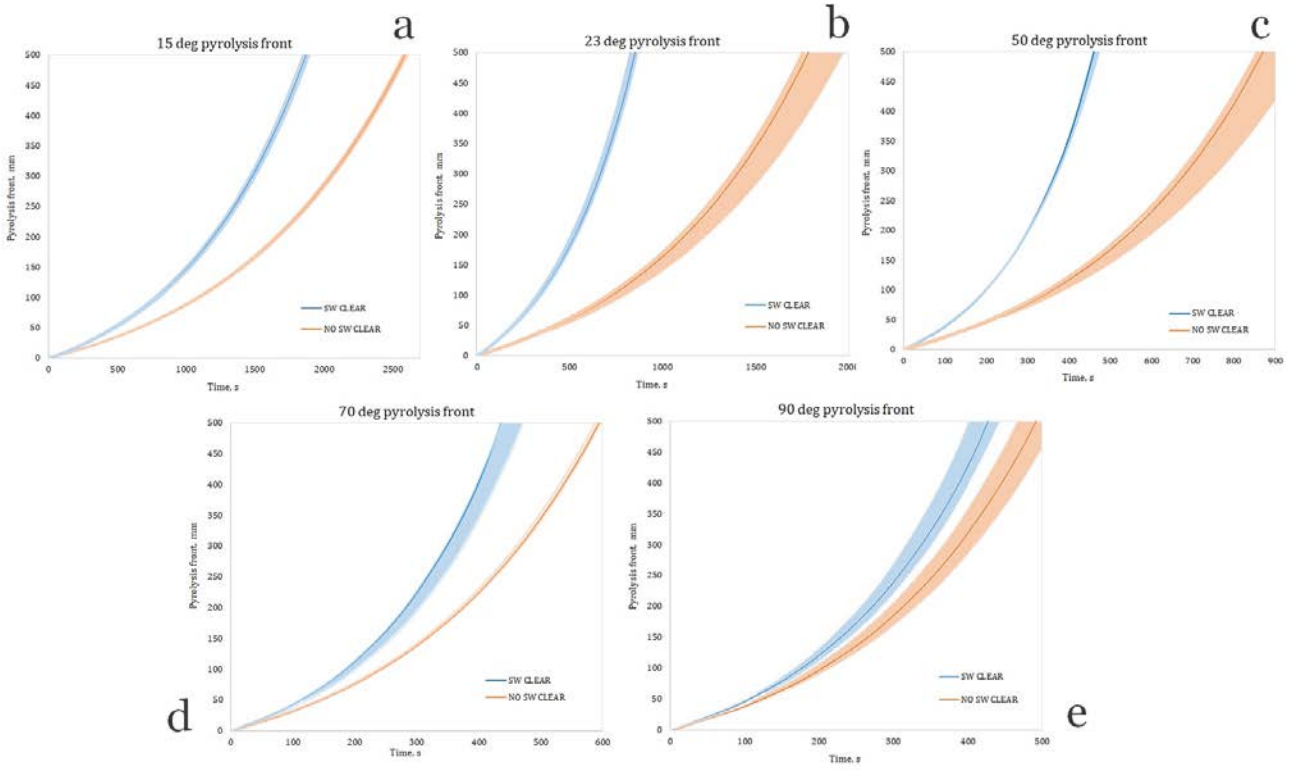

Figure 39 (a-e). Difference between trench and no trench samples at: (a) 15 degree (b) 23 degree (c) 50 degree (d) 70 degree (e) 90 degree

The most important trend that can be derived from this sequence of graphs is that the propagation of the pyrolysis front between the trench and no-trench cases are significantly different near the value of the critical angle. Also, the change is not linear since the discrepancy starts to decrease as the angle of inclination recedes from the critical value. Thus, at 23 and 50 degrees, the difference between the pyrolysis fronts seems to be the biggest among the tested angles, where the trench sample shows a much faster flame spread. However, at 70 degrees this divergence became less, reaching its minimum at the vertical position. The same happens with a 15-degree sample that shows less difference than a 23-degree sample.

3.3 Velocities and acceleration

To observe the graphical representation of how the speed and acceleration of the pyrolysis front vary at different angles of inclination, it is necessary to calculate these parameters first by using two simple formulas below:

$$V_p = \frac{x_p(t + \Delta t) - x_p(t)}{\Delta t} \tag{19}$$

$$a_p = \frac{V_p(t + \Delta t) - V_p(t)}{\Delta t} \tag{20}$$

t – the time from the first marked line, s

Δt – time is taken to pass the region between two marked lines, s

When Δt is sufficiently small, the result can be considered as a time derivative of the pyrolysis front graph. Figure 40 (a-e) shows the velocity growth as a function of the pyrolysis length that allows seeing a linear function. The graphs have the same pattern as the pyrolysis front propagation plots. Namely, at angles lower than critical, the flame spread rate has a small difference between the trench and no trench geometry, although the rate of spread in a trench is still higher.

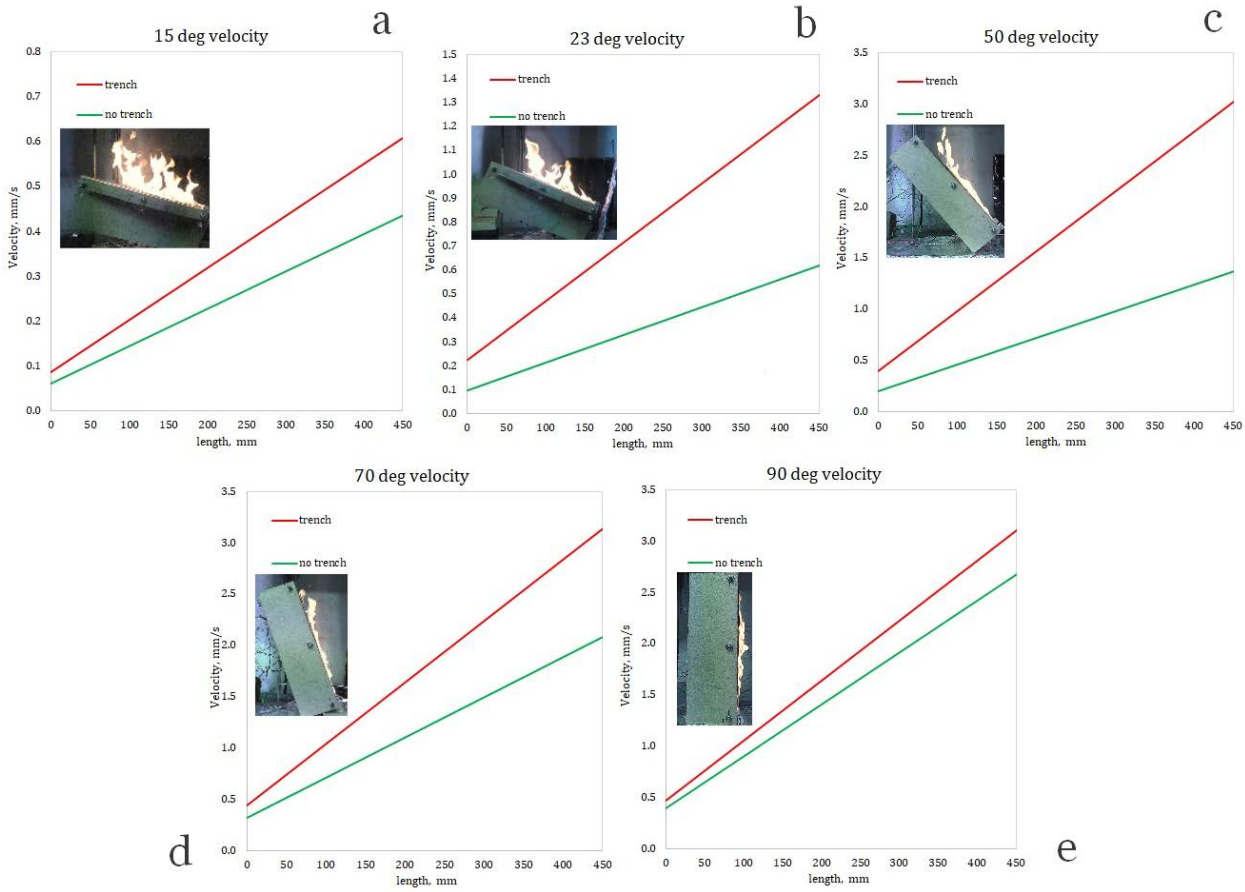

Figure 40 (a-e). Velocity graphs as a function of sample length: (a) 15 degree (b) 23 degree (c) 50 degree (d) 70 degree (e) 90 degree

From 23 to 50 degrees the difference between pyrolysis spread rates tends to increase, and finally, the closer the angle to the vertical position, the less difference in the spread rate can be observed.

To sum up the findings and finally answer the question about the presence of the vertical trench effect, it was decided to plot a graph that depicts the acceleration as a function of the inclination angle. Taking into account that the flame spread rate is always accelerative during the experiment, it would not be representative to use averaged values to plot the graphs. As an alternative, the inclination angle of the velocity graph was used from Fig. 40. Each velocity graph is described by a mathematical equation $y = kx + b$, where k is an inclination angle of a linear function. The comparison of these K-factors among each other seems to be a reasonable solution for this case. To plot the y-axis with comparable data, the highest K-value was taken as a maximal reference point for a denominator. The dimensionless ratio of K/K_{max} is denoted as a sign $Ж = K/K_{max}$ for uniformity. Thus, Figure 41 shows an acceleration distribution as the function of angle for the trench and no trench geometry.

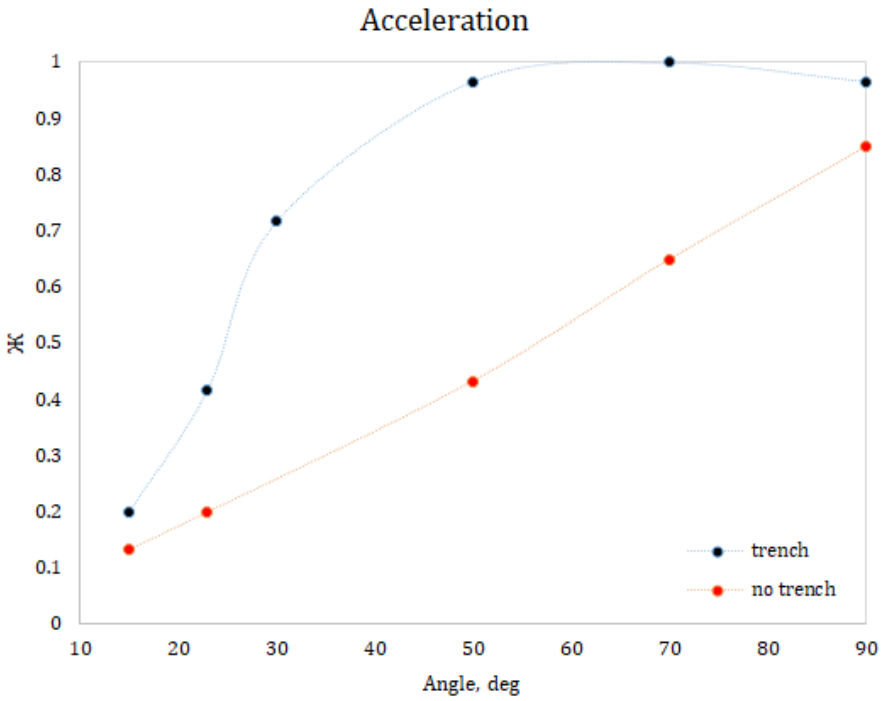

Figure 41. Change in the parameter Ж as a function of angle for acceleration

In general, the graph demonstrates a significant discrepancy between the flame spread on the trench and flat samples. The flame spread without the influence of trench walls grows almost linearly with an increase in the inclination angle. In contrast, after series of experiments with sidewalls, it became possible to reveal the trench effect that gives a completely different picture compared with the result from experiments without the sidewalls. It can be seen that the critical angle lies between 20 and 30 degrees, showing an enormous increase in acceleration.

Surprisingly, there is no significant difference in the flame spread rate at high angles from 50 to 90 degrees when the sidewalls are mounted. This also could be observed from Fig. 38 where the pyrolysis front graphs were located very close to each other, making the difference almost negligible. The value for 70 degrees is slightly higher than for 90 degrees that seems to be unrealistic. It can be explained by the presence of a human error during the early stage of the data processing that was taken into account in the pyrolysis propagation plots. Nevertheless, the flame spread rate experienced some limit, having reached the value of approximately 50 degrees. For some reason, the PMMA slab cannot be pyrolyzed more to increase the speed of the flame. In order to find a possible explanation for such a phenomenon, it would be better to look at Eq. 3 again that explains the required time for ignition of solid material that was mentioned earlier in this work. As can be seen that there are two main parameters responsible for the ignition, namely $k\rho c$

of the material and $\dot{q}_{ig}''$ heat flux going from the flames. According to Drysdale [14], the rate of the flame spread is extremely sensitive to the density of the fuel ρ with approximately $V_p \propto \rho^{-2}$ dependence. It means that combustible materials with low density (e.g. polyurethane foam) require much less heat to be pyrolyzed and then ignited. Probably in the case of PMMA, the flames are unable to provide more heat to pyrolyze more. As a consequence, the flame spread for this material is close to its limit that appeared in Fig. 41.

However, another possible and more reasonable explanation for this plateau is the strong influence of fluid mechanics. When the flames are in the trench, the pronounced flame attachment occurs at a relatively low angle of inclination. However, when the trench is inclined in between 50 and 90 degrees the flame attachment to the surface is sufficiently strong and varies only slightly. So, it means the heat flux coming to the virgin surface $\dot{q}_{ig}''$ remains approximately constant when the trench is inclined at steep angles. To understand this better, Figure 42 shows the bar chart with the time distribution for flame reaching the top of the sample and the time required for the pyrolysis front to propagate through the whole length of the slab. It can be seen that time taken by the flame to reach the top is only slightly different among angles 50-70-90, yet the fastest flame still belongs to the vertical trench. In contrast, the time taken for the flame to reach the top at 30 degrees was considerably more compared with the higher angles since the flames were marginally less attached to the surface during the test.

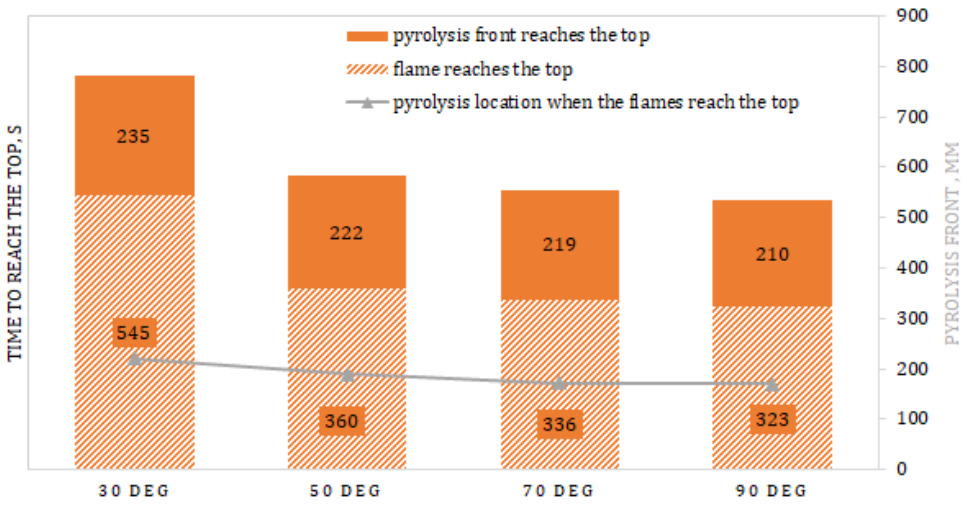

Figure 42. Time to reach the top of the sample in a trench

In contrast, acceleration without sidewalls increases continuously and the difference between the trench and no trench samples decreases considerably as the inclination angle goes higher. Nevertheless, based on the available data, the flame spread rate on a flat sample is not faster than in the trench within the same angle even if the former is in the vertical position. It can happen only if samples are wide enough that was previously discussed with Tsai et al. work [39]. So, it can be concluded that the trench effect is more pronounced at lower angles up to 50 degrees, however still exists at 90 degrees.

Furthermore, Figure 43 shows the comparison between Drysdale et al. [32] results for the flame spread rate in a trench as a function of the inclination angle and results from this work. To obtain comparable data it was decided to average the velocity from 120 mm to 420 mm since Drysdale used the same method to plot the graph. Judging by the figure, Drysdale's study mostly focused on lower angles, while this work is focused on steep angles. However, it is still possible to observe the general trend of the studies and analyze them. The first thing that should be mentioned is a good agreement in the shape of the graphs which both have a steep rise in a flame spread rate between 15 and 30 degrees.

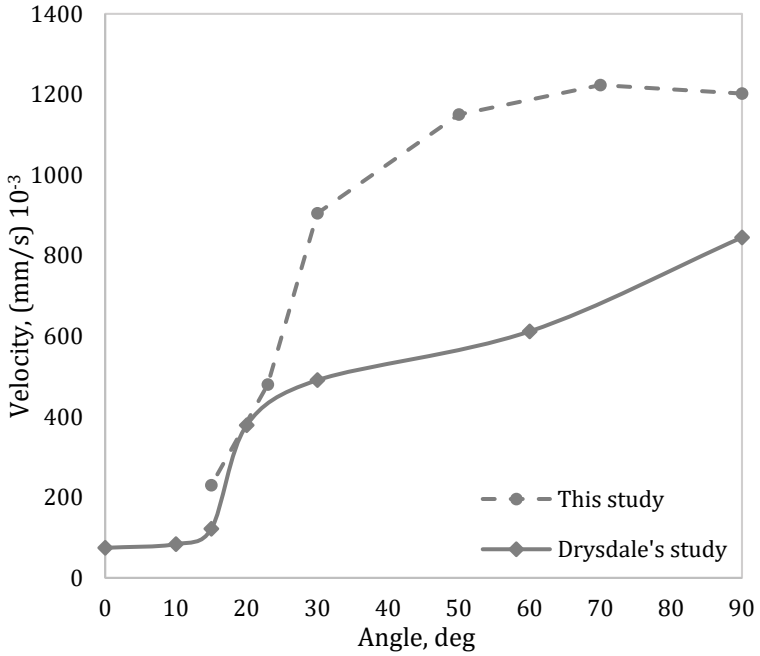

Figure 43. Comparison between Drysdale's and this study

However, after approximately 25 degrees the graphs demonstrate a very large discrepancy in the velocity distribution. To understand this difference better, Table 5 was

made in order to compare the geometrical characteristics of the trench that can greatly affect the final result.

Table 5. Difference between studies

	This work	Drysdale's study
Material of the slab	PMMA	PMMA
Length of the slab, mm	500	190
Width of the slab, mm	100	60 max
The thickness of the slab, mm	10	6
Sidewalls height, mm	100	20
Aspect ratio, A	1	0.3
Sidewall material	Vermiculite boards	Steel

From the table above it can be seen that except for the material, all geometrical parameters are very different and each component could influence the final result. For example, the sidewalls used in this study are made of vermiculite boards, while Drysdale used steel for that purpose. The heat losses to the steel walls are much higher compared with vermiculite that could change to rate of flame spread rate to the lower values. Also, the author mentioned in the conclusion that "little reliance should be placed on the 'average' rates of spread quoted for PMMA at the higher inclinations". Indeed, the discrepancy started to grow sharply after reaching the value of a critical angle after which the flame spread is concurrent. This type of flame spread is always accelerative, the longer the sample the higher velocity is expected to be in the end and as a consequence, the higher averaged velocity will be plotted on a graph. The length of the sample is more than twice longer than in the compared study and notably that the velocities are also approximately two times bigger.

Apart from that, the width of the PMMA slab plays a significant role in the flame spread rate. It should be specified that the maximum width used in Drysdale's study is 6 cm versus 10 cm in this work. According to Webster et al. study [48], the flame spread rate has a dependence on the fuel width $V_p \propto w^{0.5}$, where w is the width of the fuel sample. However, the correlation was derived for the freely suspended thermally thin cotton strips and the power of 0.5 might be inapplicable for this study. Tsai et al. [49] found out that for thermally thick PMMA slabs with sidewalls this correlation has a power of 0.35, but still the trend is upward. In another study [39] it was found that the power of the width does not depend on the fuel thickness and the presence of the sidewalls, so wider samples will produce higher flame spread rates even in a trench geometry.

3.4 Uncertainties in the pyrolysis front measurement

It is important to mention possible errors that could take place during the experiments and affect the final result. First of all, the tracking of the pyrolysis front was performed manually from the video data. This method implies a presence of error made by the subjective perception of the observer who takes readings of the front at a certain level. After several measurements of the same video file, it was calculated that the variation in the pyrolysis front location was approximately 5% at each marked line due to ambiguity in perception. Moreover, a single trial leads to some potential for statistical uncertainty. Morrisset et al. [50] found that an increasing number of tests reduces the statistical uncertainty with a relationship $1/\sqrt{n}$, where n is a number of trials. Thus, more test should be done in the future work to obtain more reliable data. In addition, the shape of the pyrolysis front varies considerably depending on the sample configuration and orientation, thus there is no apparent point that can be counted as a reference point for measurements.

Moreover, there is a possible presence of uncertainty in a sample geometry and orientation. Vermiculite board is a highly brittle material that in the case of flat samples did not ensure perfect attachment to the PMMA slab due to inherent roughness. As the consequence, the edge effect took place in the tests with flat samples, having changed the flame spread pattern.

Even though the inclination angle of the sample was measured before the test, the measurement error in combination with the influence of sidewall roughness could contribute to the total uncertainty in the results. Furthermore, the cameras used during the test have their focal length that produces some distortions in the final image. The distortion will be more feasible if the camera is installed close enough and inclined at the same time. Since the video recordings are the only source of the data, the placement has to be chosen very carefully to avoid misinterpretation of the results.

Atmospheric conditions in the laboratory certainly have a potential contribution to the uncertainty in the results. For example, when the laboratory door was opened, the incoming airflow induced an enhanced draft that influenced the flame movement when the sidewalls were absent. Also, the oxygen concentration was a variable parameter in this case due to the presence of other works that were performed during these tests.

3.5 The emissivity of the fuel

As was previously mentioned, there are two types of PMMA material used in the experiments, namely black and clear. Figure 44 (a-c) depicts the propagation of the pyrolysis front as a function of time for three angles 50-70-90 degrees.

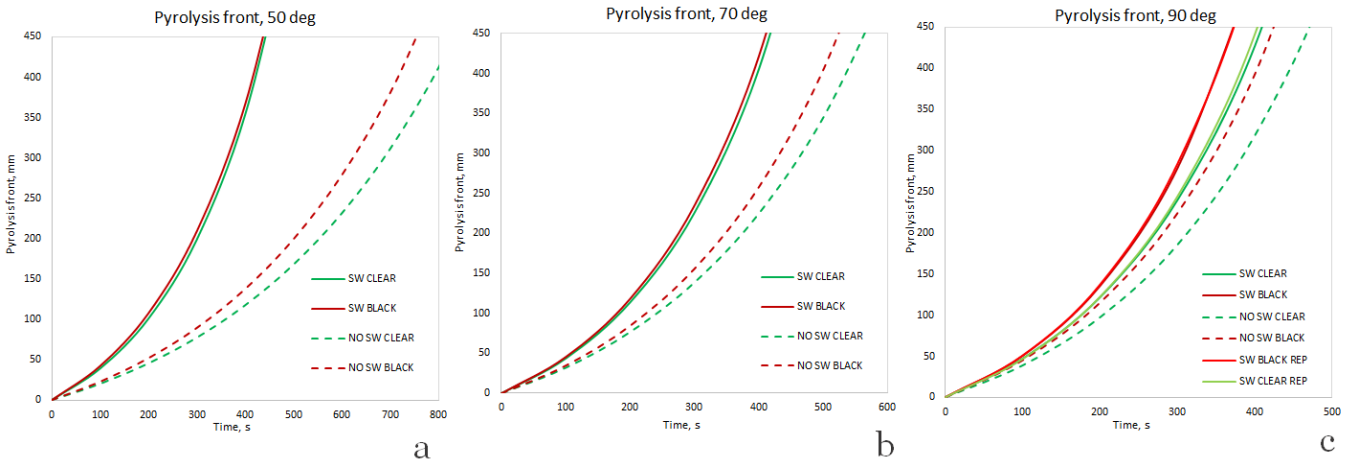

Figure 44. Pyrolysis front propagation for clear and black PMMA: (a) 50 degrees (b) 70 degrees (c) 90 degrees

From the graphs, it can be seen that the difference between black and clear trench is small for 50 and 70 degrees, while for a vertical position the discrepancy is slightly bigger but still small. To make sure that this divergence is not an error, it was decided to carry out additional tests for 90-degree black and clear trenches. Figure 44 (c) clearly shows that the results are repeatable, the lines almost coincide. Also, the results from black samples demonstrate the same trend that was observed with clear samples, the lines move closer to each other as the inclination angle goes higher. Therefore, this change seems to be independent of the material optical characteristics.

To understand the similarity between black and clear PMMA, some optical characteristics should be introduced. The total irradiation incident that interacts with a medium is expressed in the formula below [41]:

$$\rho_r + \alpha_r + \tau_r = 1 \qquad (21)$$

Yet a black PMMA sample is opaque, so the term τ tends to zero in this case. According to the Orloff et al. study [43], the emissivity of black PMMA is $\varepsilon_s = 0.95\text{-}1$, where reflectivity is also almost zero. In contrast, clear PMMA is a highly light transmitting material when it comes to discussing a visible light spectrum (400-700 nm), however for infrared radiation (700-10000 nm) the behaviour is quite distinct [51]. Referring to Figure 45 from the Plexiglas datasheet [52], which also relates to PMMA material, it

transmits most of the infrared energy from 700 to 2800 nm, except for some wavelengths depicted in the graph. However, the material becomes completely opaque (low transmittance) to infrared wavelengths from 2800 nm up to 25000 nm in thicknesses of 3 mm or greater.

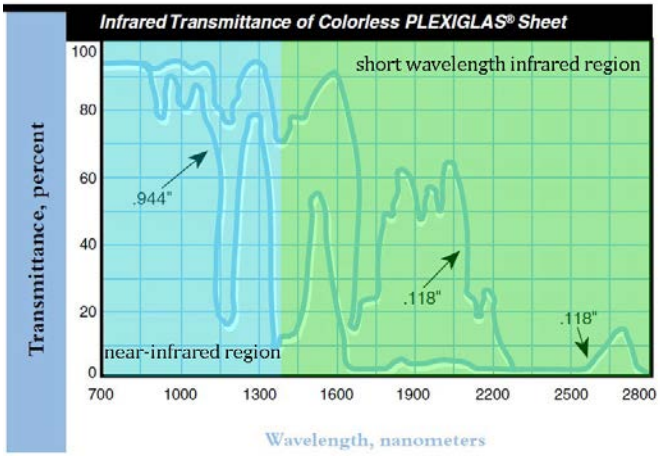

Figure 45. The transmittance of clear Plexiglas as a function of a wavelength [52]

Moreover, Hallman [53] conducted comprehensive research devoted to ignition of different plastics, where he figured out that surface radiative heat absorptance was an essential parameter in the ignition behaviour of some combustible materials. For example, Figure 46 shows a spectral absorptance of the black and clear Plexiglas as a function of a wavelength. It can be seen that black acrylic materials can almost fully absorb thermal radiation across the whole infrared band that explains its insensitivity to the type of a heating source.

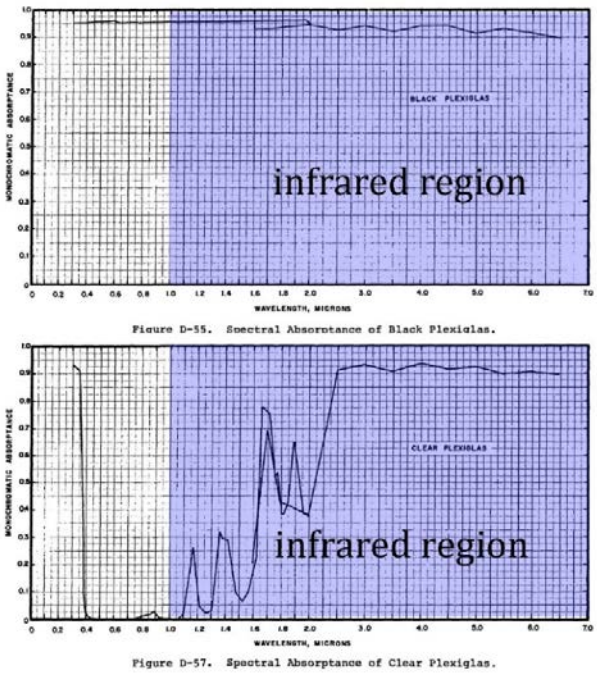

Figure 46. Absorptivity spectral dependence of black and clear Plexiglas [53]

Clear samples demonstrate a sustained high level of absorptivity only after 2500 nm. It seems that the spectral dependence can be meaningful for ignition of the PMMA in the current work since the results are surprisingly similar, despite the completely different optical characteristics.

Another example of how the spectral distribution of the heater can strongly influence the ignition of the PMMA slab was investigated by Girods et al. [54], who performed series of tests with clear PMMA samples heated by two different sources, namely a cone heater and tungsten lamps. Figure 47 (a-d) helps to understand the difference in the results. Cone heater produces radiation with a wavelength spectrum of more than 2000 nm that corresponds to a high absorptivity region of clear PMMA. Taking into account that transmittance for wavelengths over 2000 nm for thick samples is very low, active bubbling occurs only at a thin layer of the sample and material does not absorb in-depth but at the surface.

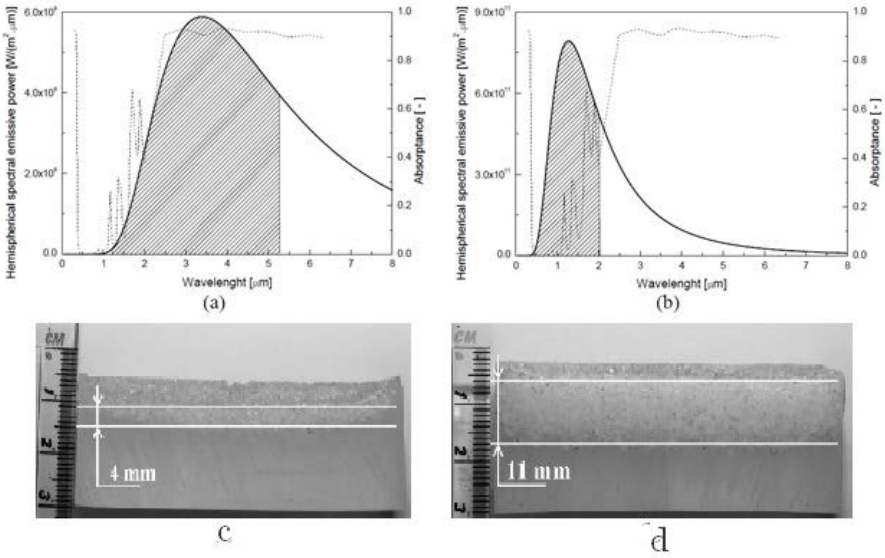

Figure 47. Dependence of the depth of the heated layer and absorptivity (a) cone heater (b)tungsten heater (c)cone heater (d) tungsten heater [54]

The clear PMMA slab heated by the tungsten heater shows considerably greater thermal penetration depth and consequently in-depth radiation that can be explained by the higher transmittance and lower absorptivity of the material at lower wavelengths, which were emitted by the radiator. Notably that in this case the temperature of the surface was lower since the lower amount of energy was absorbed and the thermal distribution across its depth was bigger.

Taking the above mentioned into consideration, it becomes evident that the burning behaviour of clear PMMA on the scales considered in these experiments is similar to black due to a specific waveband emitted by the flames. Indeed, Parent et al. [55] greatly contributed to the knowledge of the burning PMMA since they performed spectral measurements of a vertically oriented burning slab. Figure 48 depicts the radiation intensity emitted by the vertically burning 3 cm thick PMMA sample as a function of the wavenumber obtained with a spectrometer.

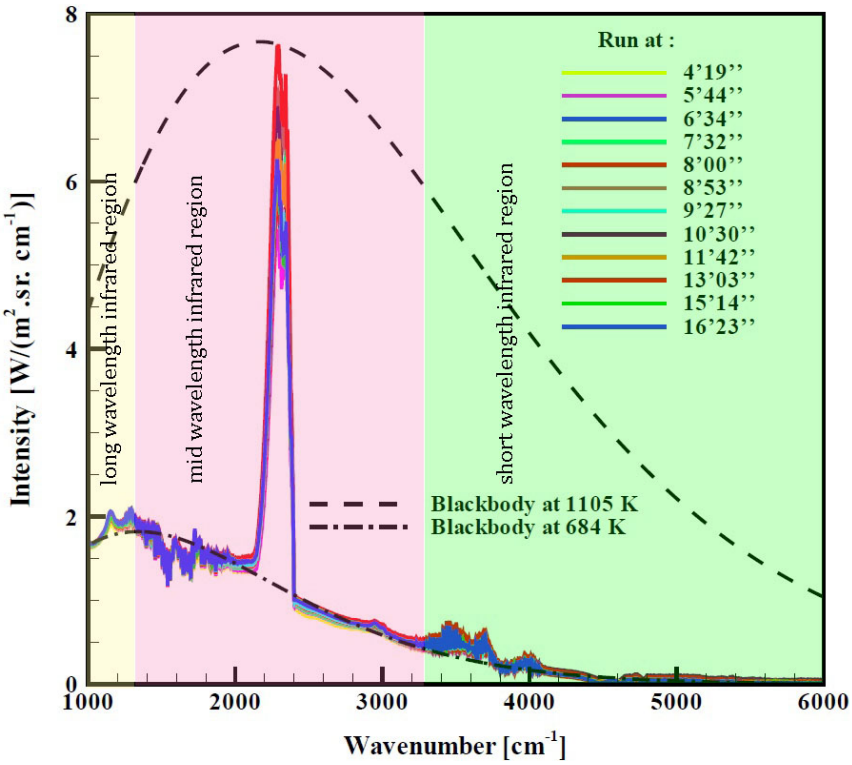

Figure 48. Radiation intensity as a function of a wavenumber [55]

In general, the most intense spectrum is located in between 1000 and 4000 cm^{-1} (10000 nm to 2500 nm), where the strongest spike is near the wavenumber of 2300 cm^{-1} (4300 nm) that can be attributed to CO and CO_2 emission in the mid-wavelength infrared region. All these wavelengths belong to the range at which clear PMMA has very low transmittance as the black PMMA, thus the ignition behaviour of clear samples is reasonably similar in his case.

Besides, the divergence between no sidewalls graphs is more substantial that can be explained by the influence of the sidewalls. The reflectivity of clear PMMA is still slightly bigger than black samples and when sidewalls are absent the reflected energy dissipates to the environment, while inside the trench it can be possibly kept inside a channel.

Last but not least, during the experimental work it was recognized that vertically oriented trenches do not have an air supply from the bottom part that could greatly affect the final result since the chimney effect might be insufficiently pronounced. Figure 49 illustrates two possible options for trench base position without a gap (a), with the gap (b), and the pyrolysis front propagation for a vertical trench with and without a gap (c). The latter demonstrates that the difference between results is negligible, so the presence of the space underside the sample is not crucial that can be taken into account in future work.

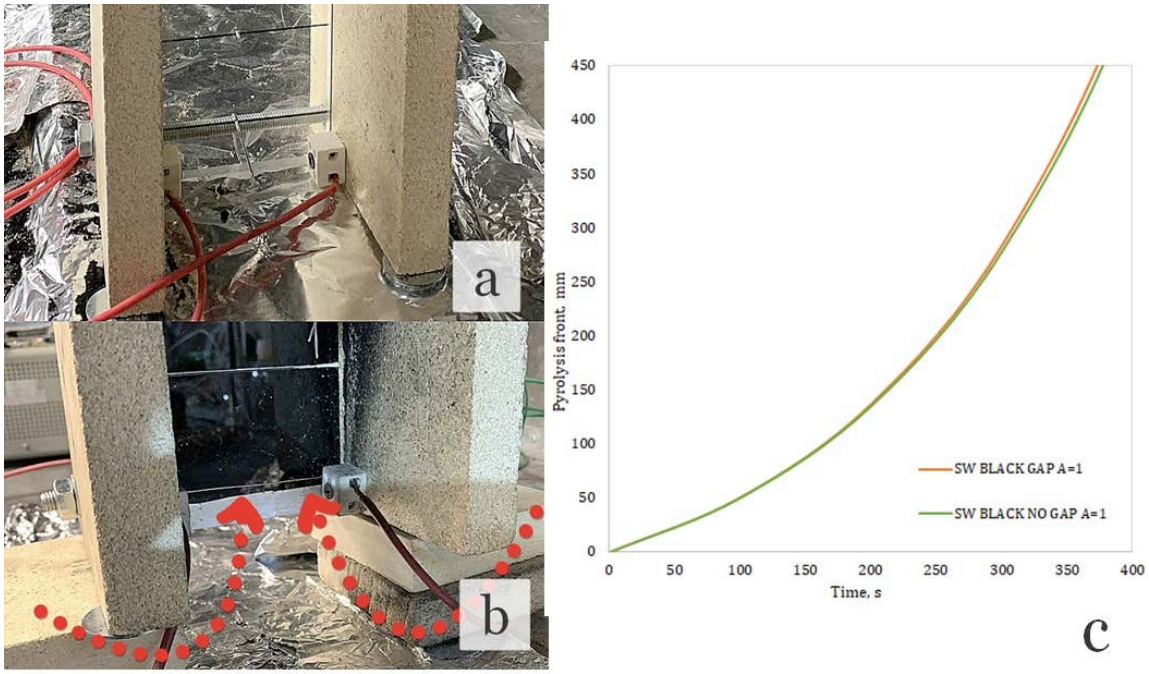

Figure 49. Trench samples with and without a gap underside (a) no gap (b) with gap (c) comparison of the pyrolysis front propagation

3.6 Aspect ratio variation

Three different aspect ratios A=H/W (A=0.5, 1, 1.5) were used in this work to examine the influence of the height of the sidewalls on the flame spread rate. Figure 50 depicts the pyrolysis front propagation as a function of time for three angles.

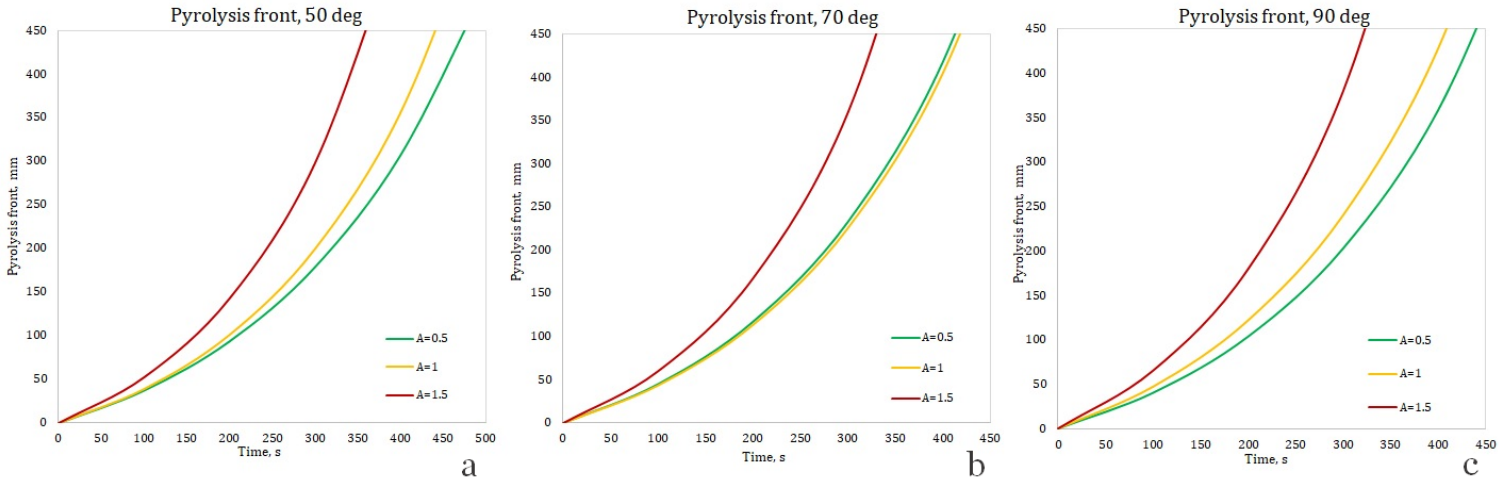

Figure 50. Pyrolysis front propagation as a function of time for different aspect ratios at (a) 50 degrees, (b) 70 degrees, (c) 90 degrees

Referring to the reviewed scope of literature, higher sidewalls produce a higher flame spread rate due to a stronger restriction of lateral entrainment, enhancement of the channeling effect and extension of the flames as a consequence. The results for the 50 and 90-degree trench are in the best agreement with the literature since the pyrolysis front propagation rate grows gradually as the aspect ratio increases. From Fig. 25 it is possible to see how the flame elongation varies with the change of the aspect ratio. As a result, longer flames give a longer preheated fuel area and a faster flame spread rate. However, at 70 degrees, the trend is not so clear since the graphs for A=1 and A=0.5 have a reversed trend compared with the other graphs. To observe the change in more detail, Figure 51 demonstrates the averaged flame spread rate as a function of the aspect ratio.

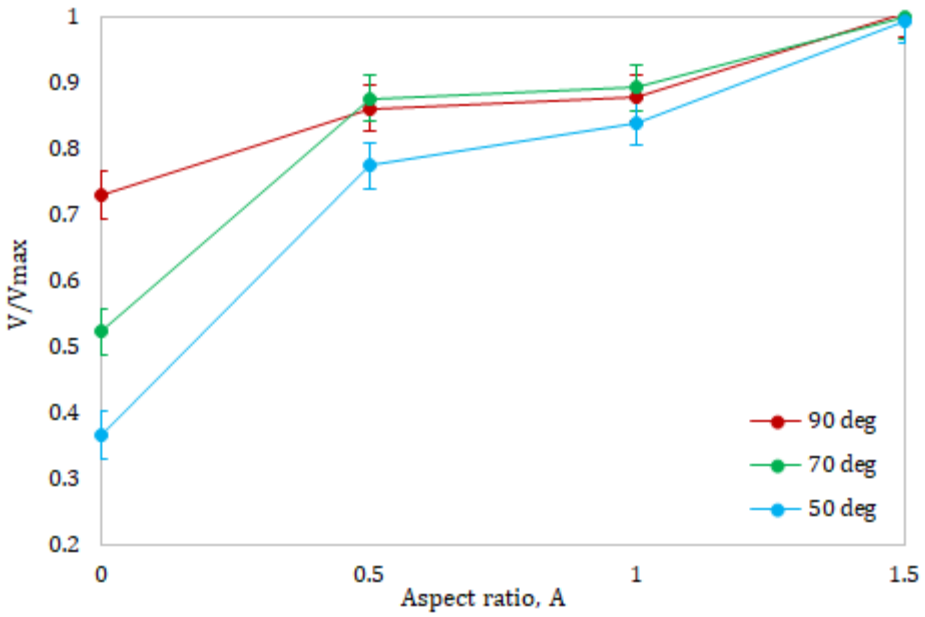

Figure 51. Velocity change as a function of an aspect ratio

The first thing that should be discussed is that the rate of flame spread for the vertical trench becomes lower than 70 degrees at A=0.5 and A=1. One of the possible reasons for such unnatural data could be an uncertainty in the inclination. While samples at lower angles were installed with a metal holder that ensured the assigned position, the vertical trench represented a self-supported structure that could have a slightly bigger inclination than 90 degrees due to an inherent roughness of vermiculite boards. According to Gollner et al. results [56], a flame spread was faster at angles slightly higher than 90 degrees, but the work was carried out on samples without sidewalls. No research has been done on the flame spread in a trench at angles more than 90 degrees that give some thoughts for future work. Moreover, human error could also take place during video data processing. Taking into account that the difference between all points at A=0.5 and A=1 is very small, even a slight error could affect the final picture. It was calculated that the average error after 3 measurements of the flame spread in the row is approximately equal to 5% that is shown in Fig. 51.

Turning to the general discussion, the trend of change is different compared with the previously mentioned An et al. study [37], who observed a gradual increase in velocity only until A=1 and then the flame spread rate on PMMA experienced a plateau for vertically oriented samples. In contrast, Yan et al. [9] investigated an upward flame spread in a trench over XPS material and observed a continuous growth from A=0 to A=1.3. In this work, the flame spread at all angles shows a plateau in between A=0.5 and A=1 and then continues to grow as the sidewalls become higher. Apart from this trend, there is another interesting pattern in the velocity change. The closer an aspect ratio to the A=1.5 the more converged lines become. When the sidewalls are absent the difference between the flame spread is tangible. Yet at aspect ratio A=1.5 the flame spread values are very similar to each other, which allows us to draw two main conclusions of this chapter. Firstly, the presence of the sidewalls greatly affects the rate of flame spread, especially at lower angles. Lastly, high sidewalls have a great influence on the formation of strong two-dimensional flow that makes flame spread rates at steep angles very similar to each other.

3.7 Temperature propagation

Since the flame spread over a thermally thick surface tends to increase perpetually and the thickness is sufficient to not reach a burnout state, the time-temperature graphs for all samples look like continuously increasing lines that should be processed for further

comparison. Figure 52 (a-b) illustrates the propagation of the pyrolysis front for samples with sidewalls (aspect ratio A=0.5) and without them and the corresponding 100°C centerline isotherms.

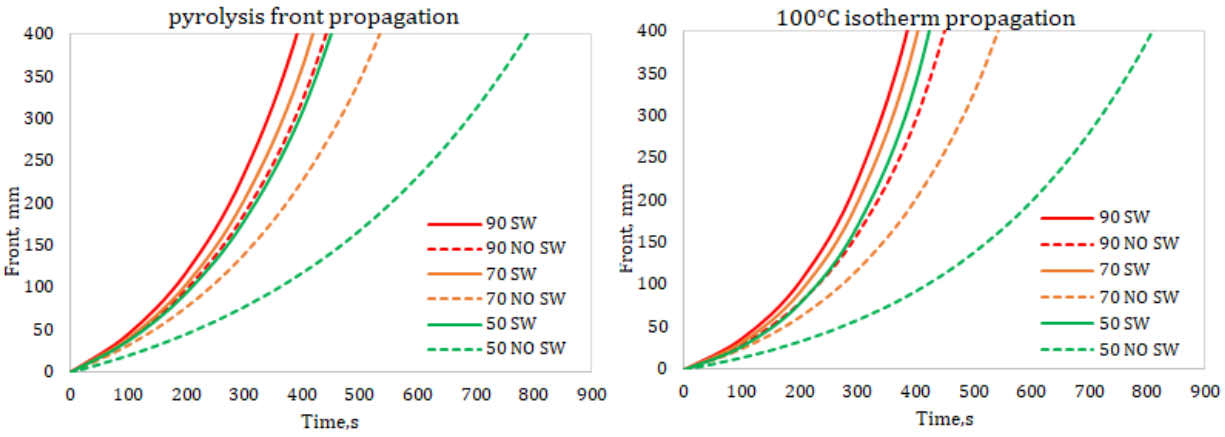

Figure 52. Pyrolysis and 100C isotherm propagation as a function of time: (a) pyrolysis (b) 100°C isotherm

The trend is consistent between both graphs, it means that the result from the video data was processed quite accurately, however, some slight discrepancies can be attributed to the error from the manual data processing. Judging by the isotherm graph, the flame spread at 50 degrees in a trench is faster than the spread at 90 degrees without sidewalls, however, the visual observation shows the reversed trend. Nevertheless, the flame spread at high angles is significantly fast both for trench and no trench, so the small differences can take place without alteration of the general picture.

To compare the results in a different way, Figure 53 depicts the relative change of the previously described term Ж as a function of angle for both pyrolysis and 100°C temperature front.

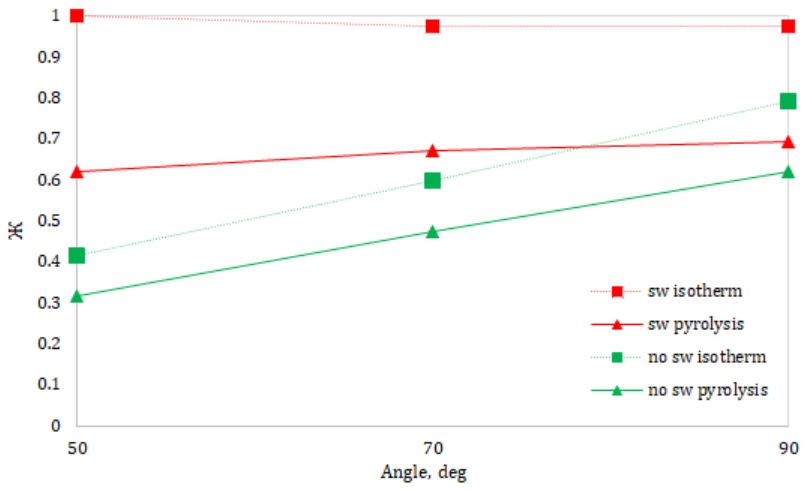

Figure 53. Velocity and 100°C isotherm change as a function of an angle

Firstly, it is straightforward to observe that velocities for the pyrolysis and temperature propagation front have the same rate of change both for the trench and no trench geometry. However, there is no variation in speed across the angles from 50 to 70 degrees for trench samples that were already shown in the chapters before with the pyrolysis front, but now the 100°C temperature velocity also confirms this plateau shape that flat samples do not show. Temperature front for samples with no sidewalls demonstrates a persistent rise until the maximal angle that was tested in this work. Apart from that, the 100°C temperature front spread rate is consistently lower than its corresponding velocity of the pyrolysis front. It possibly means that the preheating zone length always spreads faster than the pyrolysis front due to intensive preheating by the attached flame.

3.8 Uncertainty temperature measurements

Temperature results are also subjected to the uncertainty impact. As was described above, the holes for thermocouples were drilled at the equal depth of the slab thickness in order to measure the temperature in a solid phase. However, it is impossible to ensure a completely equal depth of the holes since they were drilled manually. Besides, when the PMMA slab is heated, it starts to bend towards the flame due to the material thermal expansion that affects the position of the thermocouple and its further measurements. The severity of bending depends on the angle, when it is larger the deflection of the central part becomes also larger. To mitigate this, two thin wires were passed through additional holes in the central part of the sample and fixed around the steel rod. Yet, this deflection can be also considered as a potential source of uncertainty in this work.

One more potential source of uncertainty is the vaporization temperature of PMMA that decreases with an increase of inclination angle and varies from 380°C at 10 degrees to 365°C at 90 degrees. Ito et al. [40] described this phenomenon due to the difference in heating rate. In case of downward flame spread a sample temperature is raised rapidly from ambient to its vaporization value in a short time. However, for upward flame spread, the flame front extends over the pyrolysis front and the material can be slowly heated over a long time up to its vaporization temperature.

Chapter 4 Conclusion and future work

In this work, an experimental study was performed on the topic of flame spread in a trench geometry at high angles. In addition, several experiments were conducted at lower angles to obtain a comparable general trend of a flame spread with and without sidewalls. All tests show an increase in a flame spread rate as an angle increases up to a vertical position, based on a result both from the video and temperature data. Video data analysis seems to be a very effective tool to measure the propagation of the flame spread, while temperature recordings are very sensitive to changes and prone to be less accurate results in the end. However, it is extremely important to properly incline a video camera, especially when a tested sample is inclined at lower angles since the incorrect angle can greatly distort the image.

Apart from the clear positive trend in the rate of flame spread with an increase of inclination angle, the rate of change is completely different between the trench and no trench sample. For samples with unrestricted lateral entrainment, the rate of velocity change is gradual at the range of tested angles from 15 to 90 degrees. In contrast, flame spread in a trench demonstrates the appearance of trench effect in between 15 and 30 degrees. The rate of flame spread experiences an abrupt rise that is considerably higher than the spread rate without sidewalls. Nonetheless, the rate of change in the trench tends to flatten after reaching a 50-degree value and remains roughly constant up to a vertical position. The main question of this thesis work relates to the presence of the trench effect at steep angles and it can be concluded that it still exists in the vertical position. However, the difference in flame spread rates between the trench and no trench geometry at higher angles is not so pronounced compared with results from lower angles. Yet the trench induces higher velocities for all orientations tested, so the trench effect takes place even at the vertical position. Furthermore, the results are in agreement with Drysdale's works who also revealed a sharp growth at lower angles and a much slower rate of change at higher angles. However, he focused mainly on lower angles, while this work finally contributed to the knowledge about the flame spread at steep angles.

Some important results can also be derived from the visual observation that is consistent with the graphical data. Firstly, the presence of sidewalls greatly promotes the extension of the flame length and the higher sidewalls the higher sidewalls lead to longer flame lengths. Also, the influence of the inclination angle is important especially when the

sidewalls are absent. While flames were strongly attached in a trench geometry after reaching the critical angle, flames on a flat sample demonstrated slight deflection from the surface even at steep angles that explain such discrepancies in the results from two configurations. Moreover, the shape of the pyrolysis and flame front in a trench was completely different compared with samples without sidewalls. The former showed a distinct U-shaped flame front and inverted U-shape pyrolysis front during each test due to the additional heat losses to sidewalls, the latter demonstrated triangular contour for both fronts considerably influenced by the lateral air entrainment.

In addition, several experiments were conducted where some trench parameters were varied, namely aspect ratio and emissivity of the fuel. It was discovered that aspect ratio has a feasible influence on the rate of flame spread since a higher aspect ratio produced higher flame velocities. Another important outcome is that the difference between flame spread rates at angles between 50 and 90 degrees tends to decrease with an increase of the trench aspect ratio. Thus, at the biggest tested aspect ratio A=1.5 the velocities from 50-70-90 degrees almost coincide, while at A=0 they are significantly different. In addition, both black and clear PMMA showed similar results. It was found that flames from a burning PMMA slab emit radiation mostly in the range when both clear and black material has similar optical characteristics (low transmissivity and high absorptivity) that explain very similar behaviour.

The results from this study have expanded the knowledge base for flame spread in trench environments and have shown how larger inclinations influence the occurrence of the trench effect. These findings can be used in some engineering applications, where knowledge about flame spread physics in such geometries can be crucial in terms of fire safety. Also, some questions can be potentially investigated in future research described below.

4.1 Future work

Several questions arose during the discussion of results that can be possibly taken into consideration in future studies. Firstly, no study has been done on a flame spread in a trench at angles higher than 90 degrees. There are some studies regarding an upward flame spread underneath a surface, but without restriction from two sides. Probably, the presence of sidewalls can result in completely different behaviour compared with flat samples. Secondly, black and clear PMMA materials demonstrated very similar

performance and it seems to be interesting to observe the behaviour of other materials with different density and optical parameters to accomplish the full picture of fire in a trench. In addition, it might be useful to see how sensitive a flame spread rate in a trench to external changes such as external flow, pressure and oxygen concentration. Probably, the variation of these parameters can greatly influence the speed of flame spread, revealing the most influential parameter for the case when a fire is in a channel.

References

[1] M. J. Hurley *et al.*, *SFPE handbook of fire protection engineering*, Fifth Edit. New York: Springer, 2016.

[2] Y. Zhou, R. Bu, L. Yi, and J. Sun, "Heat transfer mechanism of concurrent flame spread over rigid polyurethane foam: Effect of ambient pressure and inclined angle," *Int. J. Therm. Sci.*, vol. 155, no. March, p. 106403, 2020, doi: 10.1016/j.ijthermalsci.2020.106403.

[3] D. Fennell, "Investigation into the King's Cross Underground Fire," HSMO Books, London, 1988.

[4] K. Moodie, "The King's Cross fire: damage assessment and overview of the technical investigation," *Fire Saf. J.*, vol. 18, no. 1, pp. 13–33, 1992, doi: 10.1016/0379-7112(92)90045-E.

[5] D. X. Viegas, L. P. Pita, L. M. Ribeiro, and P. Palheiro, "Eruptive Fire Behaviour in Past Fatal Accidents," *Eighth Int. Wildl. Fire Saf. Summit, April 26-28, 2005 Missoula, MT.*, pp. 1–8, 2005.

[6] J. J. Sharples, A. M. Gill, and J. W. Dold, "The trench effect and eruptive wildfires: lessons from the King's Cross Underground disaster," in *Proceedings AFAC 2010*, 2009, no. August 2015, pp. 1–9, [Online]. Available: http://www.tathrafirebrigade.org.au/advanced/The trench effect and eruptive wildfires.pdf.

[7] C. Chen, Y. Nie, Y. Zhang, P. Lei, W. Jiao, and X. Wang, "Experimental study on flame spread over poplar plywood in inclined trench: phenomenon of flame injection," *J. Therm. Anal. Calorim.*, 2020, doi: 10.1007/s10973-020-09949-5.

[8] N. Bibby, "Mine fire kills 21 in North Eastern China," *Asia Pacific Fire*, 2015. https://apfmag.mdmpublishing.com/mine-fire-kills-21-in-north-eastern-china/ (accessed Jan. 21, 2021).

[9] W. Yan, L. Jiang, W. An, Y. Zhou, and J. Sun, "Large scale experimental study on the fire hazard of buildings' U-shape façade wall geometry," *J. Civ. Eng. Manag.*, vol. 23, no. 4, pp. 455–463, 2017, doi: 10.3846/13923730.2016.1210671.

[10] A. C. Fernandez-Pello and T. Hirano, "Controlling mechanisms of flame spread,"

Combust. Sci. Technol., vol. 32, no. 1–4, pp. 1–31, 1983, doi: 10.1080/00102208308923650.

[11] J. N. De Ris, "Spread of a laminar diffusion flame," in *Symposium (International) on Combustion*, 1969, vol. 12, no. 1, pp. 241–252, doi: 10.1016/S0082-0784(69)80407-8.

[12] F. A. Williams, *Combustion theory: The fundamental theory of chemically reacting flow systems*, Second Edi. Menlo Park, California: The Benjamin/Cummings Publishing Company, 2018.

[13] A. K. Kulkarni, "Radiative and total heat feedback from flames to surface in verticall wall fires," *Exp. Heat Transf.*, vol. 3, no. 4, pp. 397–409, 1990, doi: 10.1080/08916159008946399.

[14] D. D. Drysdale, *An Introduction to Fire Dynamics*, Third edit. Chichester, UK: John Wiley & Sons, 2011.

[15] B. Merci and T. Beji, *Fluid mechanics aspects of fire and smoke dynamics in enclosures*. London, UK: Taylor and Francis Group, 2016.

[16] A. C. Fernandez-Pello, "Flame Spread Modeling," *Combust. Sci. Technol.*, vol. 39, no. 1–6, pp. 119–134, 1984, doi: 10.1080/00102208408923786.

[17] Y. Wu, H. J. Xing, and G. Atkinson, "Interaction of fire plume with inclined surface," *Fire Saf. J.*, vol. 35, no. 4, pp. 391–403, 2000, doi: 10.1016/S0379-7112(00)00032-1.

[18] Y. Zhang, J. Ji, Q. Wang, X. Huang, Q. Wang, and J. Sun, "Prediction of the critical condition for flame acceleration over wood surface with different sample orientations," *Combust. Flame*, vol. 159, no. 9, pp. 2999–3002, 2012, doi: 10.1016/j.combustflame.2012.04.007.

[19] L. De Ris, J. Orloff, "The role of buoyancy direction and radiation in turbulent diffusion flames on surfaces," in *Symposium (International) on Combustion 15*, 1975, pp. 175–182, doi: 10.1016/s0082-0784(75)80295-5v.

[20] Y. Hasemi, "Experimental Wall Flame Heat Transfer Correlations for the Analysis of Upward Wall Flame Spread," *Fire Science and Technology*, vol. 5, no. 1. pp. 121–121, 1985, doi: 10.3210/fst.5.121.

[21] K. Saito, J. G. Quintiere, and F. A. Williams, “Upward Turbulent Flame Spread.,” in *Fire safety science-proceedings of the first international symposium*, 1986, pp. 75–86, doi: 10.3801/iafss.fss.1-75.

[22] J. Quintiere, M. Harkleroad, and Y. Hasemi, “Wall flames and implications for upward flame spread,” *Combust. Sci. Technol.*, vol. 48, no. 3–4, pp. 191–222, 1986, doi: 10.1080/00102208608923893.

[23] J. Quintiere, *Principles of fire behaviour*, Second Edi. Boca Raton: Boca Raton: CRC Press, 2017.

[24] T. P. Grumstrup, S. S. McAllister, and M. A. Finney, “Qualitative flow visualization of flame attachment on slopes,” in *10th U.S. National Combustion Meeting*, 2017, pp. 1–6.

[25] J. S. Fox and J. A. Stewart, “The Influence of Coanda Effect on Heat Transfer from Combusting Gases,” *Combust. Sci. Technol.*, vol. 19, no. 1–2, pp. 73–75, 1978, doi: 10.1080/00102207808946867.

[26] P. Woodburn and D. Drysdale, “Fires In Inclined Trenches: The Effects Of Trench And Burner Geometry On The Critical Angle,” *Fire Saf. Sci.*, vol. 5, pp. 225–236, 1997, doi: 10.3801/iafss.fss.5-225.

[27] S. Simcox, N. S. Wilkes, and I. P. Jones, “Computer simulation of the flows of hot gases from the fire at King’s Cross Underground station,” *Fire Saf. J.*, vol. 18, no. 1, pp. 49–73, 1992, doi: 10.1016/0379-7112(92)90047-G.

[28] Z. Yang and H. X. Chen, “Experimental Study on Flame Geometry along the Inclined Surface with and without Sidewalls by Using a Gas Burner,” in *Procedia Engineering*, 2018, vol. 211, pp. 925–933, doi: 10.1016/j.proeng.2017.12.094.

[29] Y. Wu and D. D. Drysdale, “Study of upward flame spread on inclined surfaces,” Sudbury, 1996.

[30] K. Moodie and S. F. Jagger, “The King’s Cross fire: Results and analysis from the scale model tests,” *Fire Saf. J.*, vol. 18, no. 1, pp. 83–103, 1992, doi: 10.1016/0379-7112(92)90049-I.

[31] X. Xie *et al.*, “Upslope fire spread over a pine needle fuel bed in a trench associated with eruptive fire,” in *Proceedings of the Combustion Institute*, 2017, vol. 36, no. 2,

pp. 3037–3044, doi: 10.1016/j.proci.2016.07.091.

[32] D. D. Drysdale and A. J. R. Macmillan, “Flame spread on inclined surfaces,” *Fire Saf. J.*, vol. 18, no. 3, pp. 245–254, 1992, doi: 10.1016/0379-7112(92)90018-8.

[33] Y. Pizzo, J. L. Consalvi, and B. Porterie, “A transient pyrolysis model based on the B-number for gravity-assisted flame spread over thick PMMA slabs,” *Combust. Flame*, vol. 156, no. 9, pp. 1856–1859, 2009, doi: 10.1016/j.combustflame.2009.06.007.

[34] J. L. Dupuy, J. Maréchal, D. Portier, and J. C. Valette, “The effects of slope and fuel bed width on laboratory fire behaviour,” *Int. J. Wildl. Fire*, vol. 20, no. 2, pp. 272–288, 2011, doi: 10.1071/WF09075.

[35] D. A. Smith, “Measurements of flame length and flame angle in an inclined trench,” *Fire Saf. J.*, vol. 18, no. 3, pp. 231–244, 1992, doi: 10.1016/0379-7112(92)90017-7.

[36] D. D. Drysdale, A. J. R. Macmillan, and D. Shilitto, “The King’s Cross fire: Experimental verification of the ‘Trench effect,’” *Fire Saf. J.*, vol. 18, no. 1, pp. 75–82, 1992, doi: 10.1016/0379-7112(92)90048-H.

[37] W. An, X. Yin, M. Cai, Y. Tang, Q. Li, and X. Hu, “Influence of U-shaped structure on upward flame spread and heat transfer behaviors of PMMA used in building thermal engineering,” *Case Stud. Therm. Eng.*, vol. 22, no. November, p. 100794, 2020, doi: 10.1016/j.csite.2020.100794.

[38] J. G. Quintiere, A. C. Carey, and L. K. Mccarthy, “Scale Modeling in Fire Reconstruction,” 2017.

[39] K. C. Tsai, “Influence of sidewalls on width effects of upward flame spread,” *Fire Saf. J.*, vol. 46, no. 5, pp. 294–304, 2011, doi: 10.1016/j.firesaf.2011.03.006.

[40] A. Ito and T. Kashiwagi, “Characterization of flame spread over PMMA using holographic interferometry sample orientation effects,” *Combust. Flame*, vol. 71, no. 2, pp. 189–204, 1988, doi: 10.1016/0010-2180(88)90007-7.

[41] T. L. Bergman, F. P. Incropera, D. P. DeWitt, and A. S. Lavine, *Fundamentals of Heat and Mass Transfer*, Seventh ed. Jefferson, USA: John Wiley & Sons, 2011.

[42] Y. Pizzo *et al.*, “Steady and transient pyrolysis of thick clear PMMA slabs,” *Combust. Flame*, vol. 162, no. 1, pp. 226–236, 2015, doi:

10.1016/j.combustflame.2014.07.004.

[43] L. Orloff, J. De Ris, and G. H. Markstein, “Upward turbulent fire spread and burning of fuel surface,” *Symp. Combust.*, vol. 15, no. 1, pp. 183–192, 1975, doi: 10.1016/s0082-0784(75)80296-7.

[44] A. Beswick and G. Rein, “Conducting Classic Fire Experiments as a showcase of Fire Safety Engineering,” Edinburgh University, 2009.

[45] T. Hirano and K. Saito, “Fire spread phenomena: The role of observation in experiment,” *Prog. Energy Combust. Sci.*, vol. 20, no. 6, pp. 461–485, 1994, doi: 10.1016/0360-1285(94)90001-9.

[46] C. Di Blasi, “Processes of flames spreading over the surface of charring fuels: Effects of the solid thickness,” *Combust. Flame*, vol. 97, no. 2, pp. 225–239, 1994, doi: 10.1016/0010-2180(94)90006-X.

[47] M. Sibulkin and J. Kim, “The dependence of flame propagation on surface heat transfer ii. upward burning,” *Combust. Sci. Technol.*, vol. 17, no. 1–2, pp. 39–49, 1977, doi: 10.1080/00102209708946811.

[48] P. H. Thomas and C. T. Webster, “Some experiments on the burning of fabrics and the height of buoyant diffusion flames,” *Fire Saf. Sci.*, vol. 420, p. 1, 1960.

[49] K. C. Tsai, “Width effect on upward flame spread,” *Fire Saf. J.*, vol. 44, no. 7, pp. 962–967, 2009, doi: 10.1016/j.firesaf.2009.06.003.

[50] D. Morrisset, G. Thorncroft, R. Hadden, A. Law, and R. Emberley, “Statistical uncertainty in bench-scale flammability tests,” *Fire Saf. J.*, vol. 122, no. March, p. 103335, 2021, doi: 10.1016/j.firesaf.2021.103335.

[51] “Electromagnetic spectrum,” *Engineering ToolBox*, 2016. https://www.engineeringtoolbox.com/electromagnetic-spectrum-d_1929.html (accessed Apr. 29, 2021).

[52] Altuglas International, “Acrylic Sheet Optical & Transmission Characteristics,” p. 12, 2000, [Online]. Available: http://www.plexiglas.com/export/sites/plexiglas/.content/medias/downloads/sheet-docs/plexiglas-optical-and-transmission-characteristics.pdf.

[53] J. R. Hallman, “Ignition characteristics of plastics and rubber,” The University of

Oklahoma, 1971.

[54] P. Girods, N. Bal, H. Biteau, G. Rein, and J. L. Torero, “Comparison of pyrolysis behaviour results between the cone calorimeter and the fire propagation apparatus heat sources,” *Fire Saf. Sci.*, pp. 889–901, 2011, doi: 10.3801/IAFSS.FSS.10-889.

[55] G. Parent *et al.*, “Radiative flux emitted by a burning PMMA slab,” in *6th European Thermal Sciences Conference (Eurotherm 2012)*, 2012, vol. 395, pp. 1–8, doi: 10.1088/1742-6596/395/1/012153.

[56] M. J. Gollner, X. Huang, J. Cobian, A. S. Rangwala, and F. A. Williams, “Experimental study of upward flame spread of an inclined fuel surface,” *Proc. Combust. Inst.*, vol. 34, no. 2, pp. 2531–2538, 2013, doi: 10.1016/j.proci.2012.06.063.

Appendix I Raw data points

50 deg											
Clear A=0.5		Clear A=1		Black A=1		Black A=1.5		Clear A=0		Black A=0	
x_p, mm	t, s	x_p, mm	t, s	x_p, mm	t, s	x_p, mm	t, s	x_p, mm	t, s	x_p, mm	t, s
70	248	70	300	70	190	70	210	70	360	70	245
120	359	120	445	120	282	120	305	120	526	120	390
170	451	170	513	170	360	170	360	170	666	170	520
220	510	220	560	220	423	220	402	220	792	220	625
270	555	270	600	270	478	270	441	270	904	270	728
320	596	320	628	320	515	320	469	320	996	320	805
370	628	370	660	370	555	370	505	370	1061	370	862
420	674	420	699	420	588	420	536	420	1107	420	930
470	715	470	741	470	608	470	566	470	1153	470	992
70 deg											
Clear A=0.5		Clear A=1		Black A=1		Black A=1.5		Clear A=0		Black A=0	
x_p, mm	t, s	x_p, mm	t, s	x_p, mm	t, s	x_p, mm	t, s	x_p, mm	t, s	x_p, mm	t, s
70	240	70	320	70	165	70	210	70	284	70	193
120	340	120	420	120	250	120	280	120	390	120	285
170	403	170	502	170	325	170	345	170	480	170	380
220	454	220	553	220	388	220	380	220	551	220	456
270	510	270	600	270	428	270	423	270	618	270	530
320	540	320	630	320	468	320	455	320	680	320	595
370	576	370	660	370	505	370	480	370	745	370	647
420	615	420	697	420	530	420	514	420	800	420	703
470	646	470	732	470	554	470	532	470	835	470	734
90 deg											
Clear A=0.5		Clear A=1		Black A=1		Black A=1.5		Clear A=0		Black A=0	
x_p, mm	t, s	x_p, mm	t, s	x_p, mm	t, s	x_p, mm	t, s	x_p, mm	t, s	x_p, mm	t, s
70	227	75	275	70	210	70	190	70	240	70	210
120	366	125	378	120	300	120	244	120	350	120	292
170	426	175	441	170	360	170	300	170	418	170	360
220	496	225	486	220	415	220	350	220	480	220	415
270	532	275	533	270	455	270	388	270	538	270	470
320	555	325	565	320	490	320	427	320	589	320	510
370	583	375	600	370	524	370	454	370	630	370	557
420	614	425	640	420	545	420	480	420	664	420	591
470	649	475	675	470	569	470	505	470	690	470	619

15 deg				23 deg				30 deg	
Clear A=1		Clear A=0		Clear A=1		Clear A=0		Clear A=1	
x_p, mm	t, s	x_p, mm	t, s	x_p, mm	t, s	x_p, mm	t, s	x_p, mm	t, s
70	685	70	860	70	245	70	630	70	255
120	1170	120	1521	120	370	120	988	120	397
170	1435	170	1900	170	492	170	1243	170	498
220	1636	220	2236	220	570	220	1483	220	567
270	1830	270	2580	270	675	270	1676	270	610
320	2010	320	2820	320	770	320	1873	320	660
370	2184			370	881	370	2026	370	698
420	2386			420	990	420	2218	420	737
				470	1058	470	2423	470	810

Appendix II Fitting curves

Angle	Config.	Aspect ratio	Material	Curve $x_p = A \cdot e^{B \cdot t}$
15	Trench	1	Clear	$y = 73.35e^{0.0011x}$
	No trench	-	Clear	$y = 72.084e^{0.0008x}$
23	Trench	1	Clear	$y = 90.83e^{0.0022x}$
	No trench	-	Clear	$y = 81.956e^{0.0011x}$
30	Trench	1	Clear	$y = 72.188e^{0.0036x}$
50	Trench	0.5	Clear	$y = 73.694e^{0.0041x}$
		1	Clear	$y = 67.046e^{0.0046x}$
		1	Black	$y = 76.385e^{0.0044x}$
		1.5	Black	$y = 73.46e^{0.0054x}$
	No trench	-	Clear	$y = 77.939e^{0.0023x}$
		-	Black	$y = 79.911e^{0.0025x}$
70	Trench	0.5	Clear	$y = 75.384e^{0.0047x}$
		1	Clear	$y = 72.978e^{0.0047x}$
		1	Black	$y = 75.878e^{0.0047x}$
		1.5	Black	$y = 76.665e^{0.0058x}$
	No trench	-	Clear	$y = 82.304e^{0.0033x}$
		-	Black	$y = 80.434e^{0.0036x}$
90	Trench	0.5	Clear	$y = 70.858e^{0.0045x}$
		1	Clear	$y = 80.734e^{0.0046x}$
		1	Black	$y = 74.101e^{0.0052x}$
		1.5	Black	$y = 86.956e^{0.0056x}$
	No trench	-	Clear	$y = 76.723e^{0.0041x}$
		-	Black	$y = 81.735e^{0.0044x}$